Terrain visibility impact on the preparation of landslide inventories: ~~some~~a practical ~~cases~~example in Darjeelig district (India)

Txomin Bornaetxea[1], Ivan Marchesini[2], Sumit Kumar[3], Rabisankar Karmakar[3], Alessandro Mondini[2]

[1]Euskal Herriko Unibertsitatea (UPV/EHU), Barrio Sarriena s/n, 48940 Leioa, Spain
[2]CNR-IRPI, via Madonna Alta 126, 06128 Perugia, Italy
[3]Geohazard Research and Management Centre, Geological Survey of India, Kolkata, India

Correspondence to: Txomin Bornaetxea (txomin.bornaetxea@ehu.eus)

Abstract. Landslide inventories are used for multiple purposes including landscape characterisation and monitoring, and landslide susceptibility, hazard and risk evaluation. Their quality/completeness can depend on the data and the methods with which they were produced. In this work we evaluate the effects of a variable visibility of the territory to map on the spatial distribution of the information collected ~~by four~~in different landslide inventories prepared using different approaches in ~~two~~a study ~~areas~~area.

The method first classifies the territory in areas with different visibility levels from the paths (roads) used to map landslides, and then estimates the landslide density reported in the inventories into the different visibility classes.

Our results show that 1) the density of the information is strongly related to the visibility in inventories obtained through fieldwork, technical reports and/or newspapers, where landslides are under-sampled in low visibility ~~classes~~areas; and 2) the inventories obtained by photo-interpretation of images suffer from a marked under representation of small landslides close to roads or infrastructures. We maintain that the proposed procedure can be useful to evaluate the quality/completeness of landslide inventories and then properly orient their use.

1 Introduction

Landslides affect the evolution of the territory and represent a hazard to the population, structures and infrastructure (Fell et al., 2008). Detailed information about the spatial and temporal distribution, and characteristics of past landslides is essential for susceptibility/hazard statistical (Hao et al., 2020; Reichenbach et al., 2018; Steger et al., ~~2016; Van~~2016a; van Den Eeckhaut and Hervás, 2012; Galli et al., 2008) and physically-based modelling (Lee et al., 2020; Park et al., 2019). ~~Complete~~However, complete landslide inventories are difficult or impossible to achieve (Corominas et al., 2014~~) and when they are~~). Inventories used~~, they~~ for basin or regional modelling should at least be statistically representative of the slope processes occurring in the studied ~~area~~areas (Cova et al., 2018; Guzzetti et al., 2012; Melzner et al., 2020).

Definición de estilo: Normal

Definición de estilo: Bullets: Esquema numerado + Nivel: 1 + Estilo de numeración: 1, 2, 3, … + Iniciar en: 1 + Alineación: Izquierda + Alineación: 0 cm + Tabulación después de: 1,27 cm + Sangría: 1,27 cm

Con formato: Fuente: 17 pto, Negrita, Color de fuente: Negro, Diseño: Claro (Color personalizado(RGB(252;252;252)))

Con formato

Con formato: Normal, Espacio Antes: 18 pto, Interlineado: Múltiple 1,83 lín., Borde: Superior: (Sin borde), Inferior: (Sin borde), Izquierda: (Sin borde), Derecha: (Sin borde), Entre : (Sin borde)

Con formato: Fuente: 17 pto, Negrita, Color de fuente: Negro, Diseño: Claro (Color personalizado(RGB(252;252;252)))

Con formato: Color de fuente: Negro, Diseño: Claro (Color personalizado(RGB(252;252;252)))

Con formato: Fuente: 12 pto, Color de fuente: Negro, Italiano (Italia)

Con formato: Color de fuente: Negro, Italiano (Italia)

Con formato: Color de fuente: Negro

Con formato: Color de fuente: Negro

Con formato: Color de fuente: Negro, Italiano (Italia)

Con formato: Italiano (Italia)

Con formato: Color de fuente: Negro

Con formato: Color de fuente: Negro

Con formato: Normal, Borde: Superior: (Sin borde), Inferior: (Sin borde), Izquierda: (Sin borde), Derecha: (Sin borde), Entre : (Sin borde), Punto de tabulación: 7,96 cm, Centrado + 15,92 cm, Derecha

Bias in sampling can prevent the ~~realization~~realisation of statistically representative inventories and introduce errors that are difficult to investigate, manage~~, propagate~~ and communicate (Guzzetti et al., 1999). ~~Largely incomplete landslide inventories can have relevant impact on derivatives products such as landslide susceptibility and hazard maps (Steger et al., 2021, 2017). Differences in~~ Lack of completeness~~ and then quality of landslide inventories~~ can largely depend on the mapping approach, the study area extent or the analysed time span, the availability of data, time and human resources (Fiorucci et al., 2018; Mondini et al., 2014; Santangelo et al., 2015). Inventories can be compiled in several ways (Guzzetti et al., 2012~~) and~~), exploiting different sources of data~~. In the case of non-automatic (or 'manual') methods which include visual interpretation of remote sensing images, direct field investigation~~, and responding to different requirements according to their usage. For example, geographical accuracy and ~~reorganisation of data inherited from historical archives a good visibility of the territory can become a key factor (Bornaetxea and Marchesini, 2021; Steger et al., 2021).~~

~~In this paper we investigate if and how the terrain visibility can limit the mapping capacity of an operator, and then influence the quality of an inventory. In other words, we compare the "data collection effect" (Steger et al., 2021) produced by the mapping of landslides in the field, with that determined by the recognition of landslides by photo interpretation of remote sensing images. In fact, Steger et al (2021) argued that the spatial distribution of landslides also depends on the "effects" generated by the adopted data collection procedure.~~

~~For this purpose, we studied a purely field-based landslide inventory available for the Gipuzkoa Province (Spain) (Bornaetxea et al., 2018), and a few inventories covering the Darjeeling district (north-east of India), obtained by interpreting several types of remotely sensed data, conducting field surveys from roads and collecting other types of information. The paper is organized as follows. In Sec. 2 we discuss the rationale behind the research. In Sec. 3 we summarize the method of the analysis while in Secs. 4 and 5 we describe the study area and the data used. Section 6 describes the visibility maps of our study areas and Sec. 7 shows the results. In Sec. 8 we discuss findings, and we draw conclusions in Sec. 9.~~

~~2 Rationale~~

~~It is widely accepted the primary role that landslide inventories play for (i) showing the location and type of landslides in a region, (ii) mapping the effects of landslide triggering events, (iii) describing the abundance of mass movements, (iv) determining the frequency-area statistics of slope failures, and (v) providing~~representativeness are relevant ~~information to train and validate landslide~~ for susceptibility ~~and/or hazard~~analysis when carried out by means of statistical models (~~Galli et al., 2008;~~ Santangelo et al., 2015; Steger et al., 2021), while occurrence dates, size and location are prioritized for damage evaluation studies, also related to climate changes (Gariano and Guzzetti, 2016). In addition, the quality and then the~~ et al., 2012). The~~ usefulness of a landslide susceptibility map is directly related to the quality of the data used to build the model (Cascini, 2008; Corominas et al., 2014; Fressard et al., 2014; Guzzetti et al., 2006; van Westen et al., 2008). The propagation of ~~the error~~errors caused by large incompleteness in ~~the~~ inventories used to produce ~~a~~ susceptibility ~~map~~maps was investigated by Steger et al. (~~2016~~2016b) and Steger et al. (2017) in Lower Austria. They discovered that biased input data ~~can~~

Con formato: Diseño: Claro (Color personalizado(RGB(252;252;252)))

Con formato: Diseño: Claro (Color personalizado(RGB(252;252;252)))

Con formato: Resaltar

Con formato: Resaltar

Con formato: Resaltar

Con formato: Resaltar

Con formato: Resaltar

Con formato: Resaltar

Con formato: Color de fuente: Negro

Con formato: Normal, Borde: Superior: (Sin borde), Inferior: (Sin borde), Izquierda: (Sin borde), Derecha: (Sin borde), Entre : (Sin borde), Punto de tabulación: 7,96 cm, Centrado + 15,92 cm, Derecha

~~generate~~generated unrealistic (or even meaningless) results, ~~and enhance the~~enhancing an apparent predictive performance of ~~a model.~~the models (Steger et al., 2021).

~~Quality requirements depend on the inventory usage. Geographical accuracy (Santangelo et al., 2015) and representativeness are relevant for susceptibility analysis when carried out by means of statistical models (Steger et al., 2021), while occurrence dates, size and location are prioritized for damage evaluation studies, also related to climate changes (Gariano and Guzzetti, 2016).~~

According to Guzzetti et al. (2012) the quality of a landslide inventory refers to the geographical and thematic information accuracy, in particular, "*completeness* ~~*(or level of completeness)*~~ *refers to the proportion of landslides shown in the inventory compared to the real (and most of the times unknown) number of landslides in the study area*". ~~Full completeness is unachievable (Corominas et al., 2014) while "*a substantially complete inventory must include a substantial fraction of the smallest landslides*" (Malamud et al., 2004). More specifically, the~~

Some authors have already suggested ways to assess quality aspects and/or completeness of an inventory ~~has often been evaluated in relation to the size of the landslides (~~. Malamud et al. (2004), starting from the work of Stark and Hovius~~,~~ (2001), focused on characteristic landslides area statistical distributions (Frequency-Area Distribution - FAD) as an indicator of completeness. Galli et al. ~~) with the expectation that the ratios between the number of landslides present in~~ (2008) suggested pairwise comparisons to rank the quality of different ~~size classes is equal or very similar to the ratios observed when considering the whole population of landslides. Guzzetti et al. (2012) stated that only event~~ inventories prepared in the same study area. Piacentini et al. ~~can be statistically representative, i.e., they contain a representative sample of the~~ (2018) analysed the spatial accuracy of an historical geospatial landslide database comparing different periods within the time laps covered by the catalogue. Trigila et al. (2010) used landslide densities in urban and non-urbanized areas to rank landslide inventories quality across the different administrative regions of Italy. Finally, Tanyaş and Lombardo (2020) proposed a completeness index for earthquake-induced landslide inventories. ~~landslide size classes, while other types of inventories can't (~~

Currently, only the approach proposed by Malamud et al~~.,~~ (2004) is commonly used in the literature as a tool to assess the completeness of inventories (e.g., Chaparro-Cordón et al., 2020; Ghorbanzadeh et al., 2019; Tanyaş et al., 2019; Zhang et al., 2019; Nicu et al., 2021; Roberts et al., 2021; Tanyaş and Lombardo, 2020; Tekin, 2021; Ubaidulloev et al., ~~).~~ 2021). However, the analysis of FADs does not include the analysis of where landslides are eventually missing in an inventory (Lima et al 2021). In fact, an inventory may show different levels of quality where the capacity of mapping of an operator changes according to the different working conditions across the study area.

Landslide inventories obtained from remotely sensed images are the most recurrent source of information used in landslide susceptibility studies at regional scale (Reichenbach et al., 2018). In the inventories produced through the interpretation of satellite or aerial images, geometric resolution of the image limits the minimum size of the landslides that can be visible and mapped by the operator in the whole scene (Guzzetti et al., 2012). ~~However, they can suffer from certain limitations related to the image's spatial resolution, the expertise of the operator (for manual and automatic classification) or the slope orientation and shadowing effects (Brardinoni et al., 2003; Jacobs et al., 2017).~~

Con formato: Resaltar

Con formato: Resaltar

Con formato: Color de fuente: Negro

Con formato: Normal, Borde: Superior: (Sin borde), Inferior: (Sin borde), Izquierda: (Sin borde), Derecha: (Sin borde), Entre : (Sin borde), Punto de tabulación: 7,96 cm, Centrado + 15,92 cm, Derecha

~~In practice, many works devoted to the landslide susceptibility/hazard zoning~~Since in this case the visibility of the territory is referred to the position of the sensor, and it can be assumed almost constant along the territory, we assume that inventories based in remotely sensed images were compiled in homogeneous working condition and then with uniform Capacity of Landslide Mapping (CoLM) over the studied area. In contrast, many scientific works were and are still based on information acquired from field surveys or from historical inventories and catalogues derived from heterogeneous information sources (Bera et al., 2019; Hussain et al., 2019; Jacobs et al., 2020; Knevels et al., 2020; Meena et al., 2019; Reichenbach et al., 2018; Rohan and Shelef, 2019; Zhang et al., ~~2019). Historical or field-based inventories often show an abundant quantity of landslides near urban areas or infrastructure, where damage is more frequent, sites are more accessible, and mitigation plans are elaborated (Guzzetti et al., 1999, 1994; Ibsen and Brunsden, 1996; Steger et al., 2021; Trigila et al., 2010; Wood et al., 2020). Usually, the accumulation of information along roads is particularly rich, highlighting that landslides and transport networks are intrinsically interconnected in terms of process and impacts (Taylor et al., 2020). The reasons of that close relationship are very complex and not fully unravelled (Brenning et al., 2015; Donnini et al., 2017; Giordan et al., 2018; McAdoo et al., 2018; Meneses et al., 2019; Santangelo et al., 2015; Sidle et al., 2014; Sidle and Ziegler, 2012), raising a need to investigate whether the major availability of roadside landslide information in inventories is purely causal (roads act as predisposing factors) or also depends on other factors, such as visibility matters.~~

~~Size~~2019). In the case of field surveys is the visual acuity, i.e. the ability of the human eye to resolve objects that occupy a small portion of the field of view, which is potentially affecting the possibility to detect landslides due to their size and/or relative position or distance respect to the operator. In fact, size, distance and orientation determine the visibility of an observed object (like a landslide) (Bornaetxea and Marchesini, 2021; Domingo-Santos et al., 2011~~). In the case of field mapping,~~) and, since, surveyors often follow predetermined roads and observe different portions of the territory from different observation points~~. Small landslides can be easily detectable if they are close to~~, the working condition changes and the ~~path, but not when they are located far away. In addition, due to their position/orientation, it~~CoLM is ~~possible that even large landslides cannot be detected. In contrast, in a satellite or aerial image,~~not-uniform over the ~~visibility~~surveyed area. This study presents a framework to assess where and how the point of observation of the ~~territory is referred to the position of~~operator affects the ~~sensor, and it can be assumed to be almost constant and homogeneous, even though spatial resolution and geometric acquisition may limit the minimum size of landslides that can be detected (Mondini et al., 2014). Therefore,~~CoLM uniformity, and hence the quality ~~and~~ /completeness of ~~an~~the inventory ~~can be intrinsically linked to the data acquisition method.~~ .

The method is based on the concept of “estimated visibility” (EV), which is a computer-based simulation of the real visibility of an object from a point of observation, and on the measure of the spatial landslide density in an area related to the EV. We tested the proposed framework using three inventories available for the Darjeeling district (north-east of India) and prepared with different data and methods including field-based surveys, aerial and satellite photo-interpretation.

Con formato: Diseño: Claro (Color personalizado(RGB(252;252;252)))
Con formato: Diseño: Claro (Color personalizado(RGB(252;252;252)))
Con formato: Diseño: Claro (Color personalizado(RGB(252;252;252)))
Con formato: Diseño: Claro (Color personalizado(RGB(252;252;252)))
Con formato: Diseño: Claro (Color personalizado(RGB(252;252;252)))
Con formato: Diseño: Claro (Color personalizado(RGB(252;252;252)))
Con formato: Diseño: Claro (Color personalizado(RGB(252;252;252)))
Con formato: Diseño: Claro (Color personalizado(RGB(252;252;252)))
Con formato: Diseño: Claro (Color personalizado(RGB(252;252;252)))
Con formato: Diseño: Claro (Color personalizado(RGB(252;252;252)))
Con formato: Diseño: Claro (Color personalizado(RGB(252;252;252)))
Con formato: Diseño: Claro (Color personalizado(RGB(252;252;252)))
Con formato: Color de fuente: Negro
Con formato: Normal, Borde: Superior: (Sin borde), Inferior: (Sin borde), Izquierda: (Sin borde), Derecha: (Sin borde), Entre : (Sin borde), Punto de tabulación: 7,96 cm, Centrado + 15,92 cm, Derecha

2 Study area

We applied the approach in an area of ~513 km² within the Darjeeling district, the northernmost district of West Bengal state (north-east of India) (Fig. 1). The area starts just above the foothills of Himalaya in the south and goes beyond the Higher Himalayas in the north. The area lies within the highly dissected hill ranges of the sub to higher Himalayas with elevation varying from 200 m to 2900 m. About 48% of the area has slopes between 15° and 30°, however the steeper slopes are mainly restricted in the escarpment or cliffs present in the area. The major part of the area is covered by Tea plantation (39%), followed by Moderate vegetation (24%), Sparse vegetation (19%), Thick vegetation (8%), Settlement and Cultivated land (4% each). The area is a part of active fold thrust belt of Darjeeling Himalayas where sedimentary rocks of Sub-Himalayas, low grade meta-sedimentaries of lesser Himalayas and high-grade rocks of Higher Himalayas are present with or without the overburden cover of varied thickness. These sequences of different grades of rocks are separated by E-W trending major tectonic features like Himalayan Frontal Thrust (HFT), Main Boundary thrust (MBT) and its splay as well as Main Central Thrust (MCT). The area is located within the seismic Zone-IV of seismic zonation map of India.

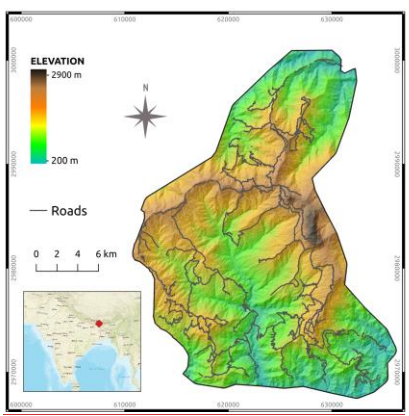

Figure 1: Location map of Darjeeling district (India) - Projection: WGS 84 / UTM zone 45N, Location Base Maps: © OpenStreetMap contributors 2021. Distributed under the Open Data Commons Open Database License (ODbL) v1.0.

The Darjeeling study area experiences a temperate climate with wet summers which gradually moves into monsoon season when the area receives a number of wet spells, notorious for triggering landslides. This part of the Eastern Himalayas receives the maximum amount of precipitation within the entire Himalayas.

The Darjeeling Himalayas is perennially landslide-prone and frequently experiences landsliding events of variable magnitudes. Most of these landslides are triggered by incessant monsoon rain between June and September, with some occasional major landsliding events in between.~~Some authors have suggested ways to assess the quality and/or the completeness of an inventory. Malamud et al. (2004) proposed the landslides area statistical distribution (Frequency-Area Distribution - FAD) as an indicator~~

Con formato: Fuente: 9 pto, Negrita

Con formato: Normal, Espacio Después: 10 pto

Con formato: Color de fuente: Negro

Con formato: Normal, Borde: Superior: (Sin borde), Inferior: (Sin borde), Izquierda: (Sin borde), Derecha: (Sin borde), Entre : (Sin borde), Punto de tabulación: 7,96 cm, Centrado + 15,92 cm, Derecha

~~of completeness, which was used by many authors (e.g., Chaparro-Cordón et al., 2020; Ghorbanzadeh et al., 2019; Tanyaş et al., 2019; Zhang et al., 2019). According to Malamud et al. (2004), the inverse gamma distribution can be used to model the frequency density of landslide sizes in an inventory. A number of authors consider an inventory statistically representative only for landslides larger than the roll-over value (Nicu et al., 2021; Roberts et al., 2021; Tanyaş and Lombardo, 2020; Tekin, 2021; Ubaidulloev et al., 2021). Galli et al. (2008) suggested a framework, based on pairwise comparisons (geographical abundance, cartographic matching, frequency area statistics, and effectiveness in modelling landslides), to rank inventories prepared in the same study area. Piacentini et al. (2018) analysed the spatial accuracy of a historical geospatial landslide database comparing different periods within the time laps covered by the catalogue. They also verified the completeness of the database by the conventional FAD analysis. Trigila et al. (2010) used landslide densities in urban and non-urbanized areas to rank landslide inventories quality across the different administrative regions of Italy. Setting a buffer of 750 m around the urban areas they ranked higher those inventories where the percentage of landslides mapped outside the buffer areas was larger. The approach requires the choice of a fixed buffer a-priori not connected to the local morphology of the area, to the related geomorphological processes and to the visibility of the slopes from urban centres. Finally, Tanyaş and Lombardo (2020) proposed a completeness index for earthquake-induced landslide inventories. The index is a function of the Peak Ground Acceleration values and therefore cannot be applied to rain-induced landslide inventories or historical archives.~~

~~In this work we analyse the possible relationship between the degree of visibility of the territory from roads and the spatial distribution of information on landslides contained in 4 inventories, prepared with different data and methods. In other words, the "data collection effect" (sensu Steger et al. (2021)), on different types of inventories, is investigated and discussed.~~

Notice that in Darjeeling roads are usually positioned along the relief's ridges (Fig. 1).

3 Methods and Data

3.1 Methods

Estimated visibility (EV) simulates the visibility of an object from an observation point. In this paper ~~we estimated~~ EV is measured by the "solid angle" (SA - unit of measurement: square minutes [min^2]), a metric that quantifies the level of visibility of ~~the territory using roads as observation points for the inventories obtained through field investigation and we assumed constant visibility when remotely sensed images were used.~~

~~For field-based maps, we used the solid angle (SA) metric as~~ an object, of known size and orientation, located at a certain distance from an observer or, in other words, a ~~measure of the visibility of an object. SA value~~metric that measures the portion of the observer field of view occupied by ~~the~~an object.

~~We calculated SA maps using~~ We intend here the visibility of a landslide as the portion of the field of view of an observer occupied by the landslide itself, and we estimate it (Estimated Visibility, or EV) through the relative solid angle (SA) in square

Con formato: Color de fuente: Negro

Con formato: Normal, Borde: Superior: (Sin borde), Inferior: (Sin borde), Izquierda: (Sin borde), Derecha: (Sin borde), Entre : (Sin borde), Punto de tabulación: 7,96 cm, Centrado + 15,92 cm, Derecha

minutes [min^2]. The apex is the point from which the slope is observed and the landslide subtends its solid angle from that point. EV depends then from the size and the orientation of the slope/landslide, and the distance.

We used r.survey to simulate the EV (Bornaetxea and Marchesini, 2021). r.survey is an open source spatial analysis tool useful to assess how the terrain morphology is perceived by an observer located at a defined observation point, or a group of points. It was designed for evaluating the visibility of features lying on the terrain slopes, including landslides. ~~The positions of the observer, a DTM and the size of the target object whose visibility is going to be assessed (a landslide in this case) are the mandatory inputs.~~ Among the different outputs, the tool provides the map of the maximum solid angle (SA). In the maximum solid angle map, each pixel has only one value. However, each pixel is potentially observed from several observation points. Here, the pixel value represents the maximum solid angle value calculated among all observation points from which the pixel is visible. SA value depends on the size of the observed object, the distance (between observers and target) and the relative orientation of the target with respect to the observation point.

The data required to ~~obtain SA~~run r.survey are a ~~digital terrain model,~~Digital Terrain Model (DTM), a landslide inventory, and a set of points of observations.

In this work, during the field surveys, the surveyors mainly travel on roads. Consequently, the simulation of visibility was performed starting from the road ~~map. First~~network. For this purpose, we generated a set of closely spaced points along the roads~~. These points redundantly~~ to simulate the observation points of a surveyor moving along the roads. Then we used r.survey to calculate the maximum SA map for a circular object, similar in size to the smallest landslide in the inventory. ~~After that, we obtained the visibility class map (SAc) by thresholding the~~The SA values~~.~~ were then collapsed into SA classes in order to obtain an EV map. Additionally, we ~~smoothed~~filtered the ~~SAc maps,~~EV map by replacing the central pixel values with the most frequent class (mode) in a 3x3 moving window, in order to remove isolated pixels belonging to different classes with respect to the surrounding ones. Finally, we estimated the landslide density counting the number of landslides in each ~~visibility~~SA class. Since landslides are commonly collected as polygonal areas, it may happen that a single landslide overlaps more than one ~~visibility~~SA class. In this case, we assigned the landslide to the most present class within the landslide polygon.

We used two metrics to measure the spatial density: the Normalized Landslide Count (NLC) and the Standardized Landslide Density (SLD).

We used NLC to compare the spatial density of landslides included in different inventories prepared for the same study area (Eq. 1):

$$NLC_i = \frac{n_i}{n_t}, \quad (1)$$

where n_i and n_t represent the number of landslides in the SA class i and the total number of landslides, in the inventory, respectively.

~~We~~Alternatively, we used SLD (Eq. 2) to compare the spatial density of landslides ~~included in different~~ inventories prepared for different study areas (~~Eq. 2~~see section 4.3):

$$SLD_i = \frac{NLC_i}{(A_i/A_t)}, \quad (2)$$

Con formato: Color de fuente: Negro

Con formato: Normal, Borde: Superior: (Sin borde), Inferior: (Sin borde), Izquierda: (Sin borde), Derecha: (Sin borde), Entre : (Sin borde), Punto de tabulación: 7,96 cm, Centrado + 15,92 cm, Derecha

where A_i and A_t are respectively the area of ~~visibility~~SA class *i* and the total area.

The SLD metric normalises NLC according to the percentage of territory occupied by the ~~visibility~~SA classes. These percentages, in fact, can be slightly different among the study areas, due to the smoothing performed to remove isolated pixels. The entire flowchart is described in Fig. ~~1~~2.

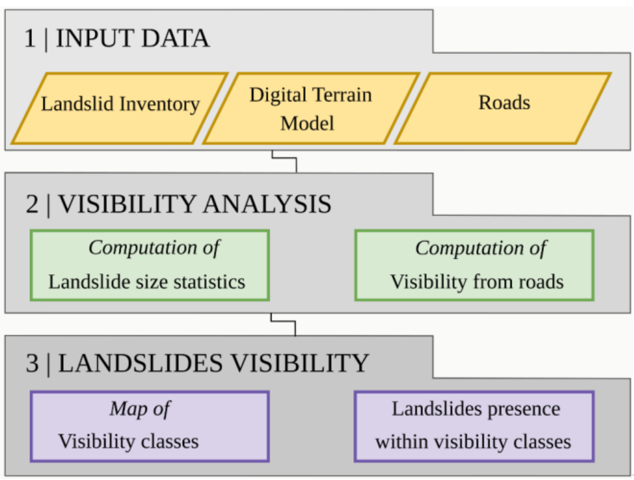

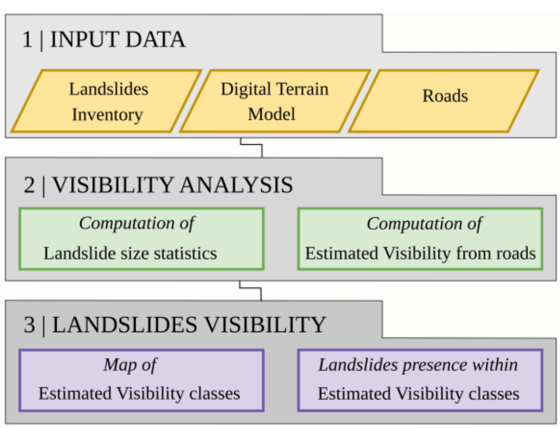

Figure ~~1~~2: Conceptual-chart illustrating the proposed GIS-based approach.

Con formato: Fuente: 9 pto, Negrita, Color de fuente: Negro

Con formato: Fuente: 9 pto, Negrita, Color de fuente: Negro

Con formato: Color de fuente: Negro

Con formato: Normal, Espacio Después: 10 pto, Borde: Superior: (Sin borde), Inferior: (Sin borde), Izquierda: (Sin borde), Derecha: (Sin borde), Entre : (Sin borde)

Con formato: Color de fuente: Negro

Con formato: Normal, Borde: Superior: (Sin borde), Inferior: (Sin borde), Izquierda: (Sin borde), Derecha: (Sin borde), Entre : (Sin borde), Punto de tabulación: 7,96 cm, Centrado + 15,92 cm, Derecha

~~**4 Study areas**~~

~~We first tested the approach in Gipuzkoa Province. It is a ~1980 km² region located in the north of the Iberian Peninsula, along the western end of the Pyrenees (Fig. 2a). It is lithologically heterogeneous, with deposits dated from Paleozoic to Quaternary, and presents the typical hilly and mountainous Atlantic landscape. The average annual precipitation is 1597 mm, with two maximum seasons: November–January and April. More detailed description about this study area can be found in (Bornaetxea et al., 2018).~~

~~We applied the same approach in an area of ~513 km² within the Darjeeling district, the northernmost district of West Bengal state (north-east of India) (Fig. 2b). The area starts just above the foothills of Himalaya in the south and goes beyond the Higher Himalayas in the north. The area lies within the highly dissected hill ranges of the sub to higher Himalayas with elevation varying from 200 m to 2900 m. About 48% of the area has slopes between 15° and 30°, however the steeper slopes are mainly restricted in the escarpment or cliffs present in the area. The major part of the area is covered by Tea plantation (39%), followed by Moderate vegetation (24%), Sparse vegetation (19%), Thick vegetation (8%), Settlement and Cultivated land (4% each). The area is a part of active fold thrust belt of Darjeeling Himalayas where sedimentary rocks of Sub-Himalayas, low grade meta-sedimentaries of lesser Himalayas and high-grade rocks of Higher Himalayas are present with or without the overburden cover of varied thickness. These sequences of different grades of rocks are separated by E-W trending major tectonic features like Himalayan Frontal Thrust (HFT), Main Boundary thrust (MBT) and its splay as well as Main Central Thrust (MCT). The area is located within the seismic Zone-IV of seismic zonation map of India (BIS 2002).~~

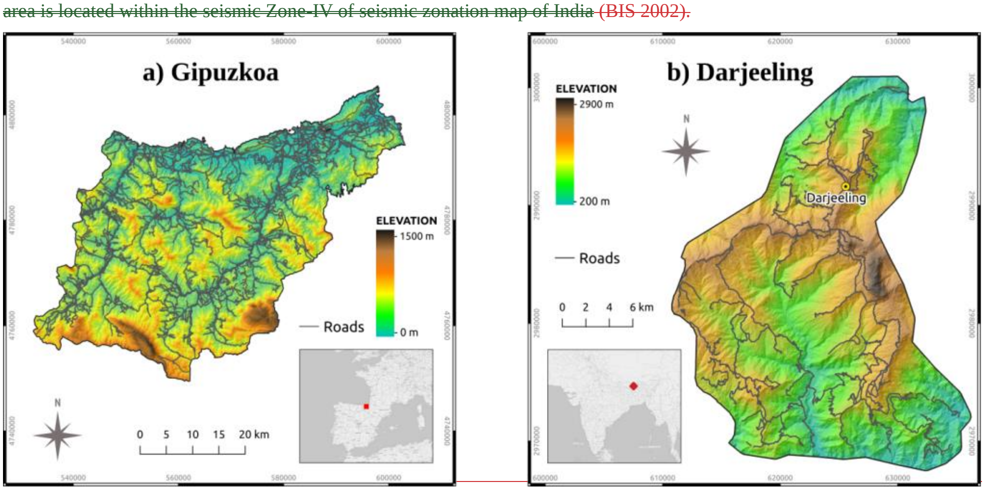

~~Figure 2: Location maps of Darjeeling district (India) - Projection: WGS 84 / UTM zone 45N - and Gipuzkoa province (Spain) – Projection: ETRS89 / UTM zone 30N.~~ ~~**Location Base Maps: © OpenStreetMap contributors 2021. Distributed under the Open Data Commons Open Database License (ODbL) v1.0.**~~

Con formato: Normal, Espacio Después: 10 pto

Con formato: Fuente: 9 pto, Negrita

Con formato: Color de fuente: Negro

Con formato: Normal, Borde: Superior: (Sin borde), Inferior: (Sin borde), Izquierda: (Sin borde), Derecha: (Sin borde), Entre : (Sin borde), Punto de tabulación: 7,96 cm, Centrado + 15,92 cm, Derecha

~~The Darjeeling study area experiences a temperate climate with wet summers which gradually moves into monsoon season when the area receives a number of wet spells, notorious for triggering landslides. This part of the Eastern Himalayas receives the maximum amount of precipitation within the entire Himalayas.~~

~~The Darjeeling Himalayas is perennially landslide-prone and frequently experiences landsliding events of variable magnitudes. Most of these landslides are triggered by incessant monsoon rain between June and September, with some occasional major landsliding events in between.~~

~~Study areas road networks are shown in Fig. 2. In Gipuzkoa roads are mostly located along the valleys while in Darjeeling roads are usually positioned along the relief's ridges.~~

~~5~~3.1 Data

~~For Gipuzkoa Province, we used a landslide inventory prepared, by one of the authors, during the field-work campaign carried out in the period from June to August 2016 (Bornaetxea et al., 2018). We cleaned the database from landslides not detected by means of visual inspection on the field, and 542 shallow landslides remained~~The~~. This inventory is referred to as **Gipuzkoa inventory**. Additionally, the map of the roads followed during the field-work campaign and 5 meters resolution DTM was available. For the Darjeeling study area, the~~ Geological Survey of India (GSI) provided us with an inventory that was the result of a field-work campaign carried out after the monsoon period (that goes from June to September) of 2019. This inventory, named **GSI Field**, provides ~~landslide~~landslides locations as points~~, so the FAD curve cannot be computed.~~. Additionally, GSI also provided us with a historical landslide inventory (**GSI Historic**) for the Darjeeling area. It is a multi-temporal landslide inventory devoted to landslide susceptibility modelling and studying triggering mechanisms, landslide domains and mitigation actions. This database gathers information about landslides that have occurred since 1968. As it usually occurs with national or regional multi-temporal databases (~~Van~~van Den Eeckhaut and Hervás, 2012), the information in this data-base is heterogeneous. Out of 1240 landslides, 80% are represented as polygons, while 20% are single points. Almost half of the landslides (47.6%) were mapped by means of satellite image photo-interpretation, using the available images coming from diverse sources, such as Cartosat PAN (2~~%),~~%) (2.5m x 2.5m), LISS IV (1%) (5.8m x 5.8m) and Google Earth or other base satellite maps available in ESRI's ArcGIS 10.2 (44.6%). The rest of the data came mainly from legacy data, including data collected from GSI reports, and Toposheet (34.6%). The latter corresponds to a Topobase map of Survey of India (SOI) surveyed in 1969-70 at 1:25000 scale. Other sources such as Darjeeling Himalayan Railway's database (7.5%), Blogs or Newspapers (3.5%) and Field-work (6.8%) complete the available information. Debris slides (69.43%) and rock slides (18.4%) are the most frequently reported failures together with debris flows (5.3%), rock fall (0.23%), deep rotational slides (1.95%) and unknown (4.69%). ~~We named this inventory as **GSI Historic**. We obtained the corresponding FAD curve only using the landslides mapped as polygons. The curve (Fig. 3) shows the conventional power-law fit with a relatively low roll-over (Malamud et al., 2004).~~ Lastly, we mapped landslides triggered by the 2019-2020 monsoon season using a pre-event pan sharpened Spot 6 image acquired on 22th March of 2019 and a pan sharpened post-event image acquired on 3th April of 2020

Con formato: Título 2

Con formato: Color de fuente: Negro

Con formato: Normal, Borde: Superior: (Sin borde), Inferior: (Sin borde), Izquierda: (Sin borde), Derecha: (Sin borde), Entre : (Sin borde), Punto de tabulación: 7,96 cm, Centrado + 15,92 cm, Derecha

by the same satellite. We used the two 2.5 x 2.5 m spatial resolution images to detect landslides occurring in between the two acquisitions following a photo interpretation approach. In this inventory, referred to as **Spot 2020**, we classified most of the landslides (95%) as earth and debris flows, and the rest as complex movements. Figure 3 shows ~~the~~ that GSI Historic and Spot 2020 FAD curves reveal a power law shape ~~of the FAD curve~~ on the right of the rollover ~~and a low rollover~~ value (Malamud et al., 2004). ~~Table 1 summarizes the~~ The FAD curve could not be computed for GSI Field inventory due to the absence of the information about the ~~four~~landslide sizes. Fig. 3 also describes some characteristics of the available inventories.

In addition to the landslide information, GSI also provided us with the road network map of Darjeeling, together with the 10x10 meters resolution DTM.

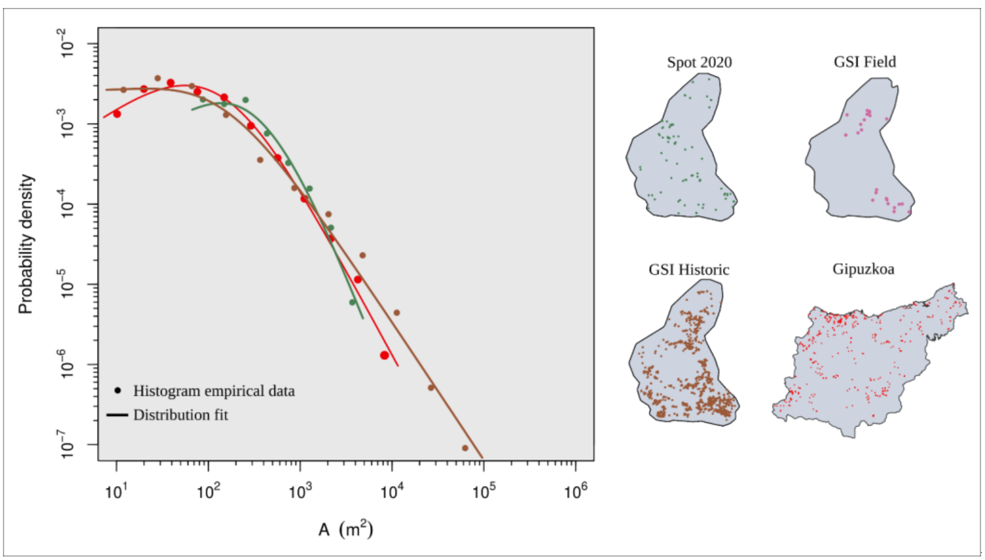

Con formato: Color de fuente: Negro

Con formato: Normal, Borde: Superior: (Sin borde), Inferior: (Sin borde), Izquierda: (Sin borde), Derecha: (Sin borde), Entre : (Sin borde), Punto de tabulación: 7,96 cm, Centrado + 15,92 cm, Derecha

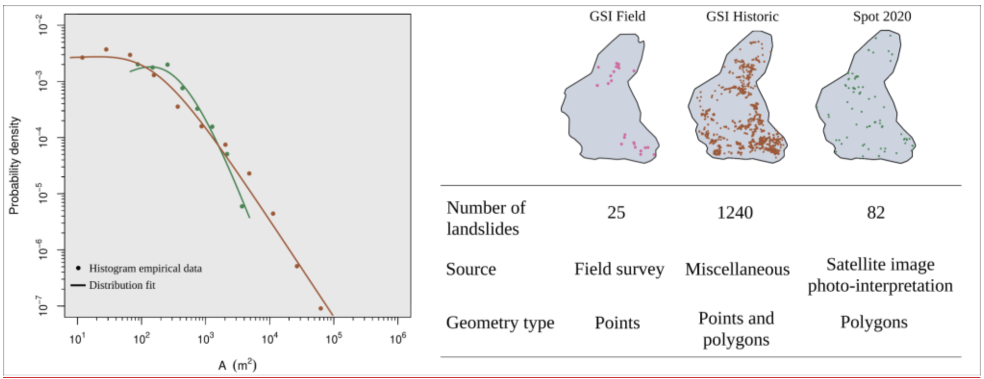

Figure 3: Frequency area distribution curves (FAD curves) for Spot 2020 (green), GSI Historic (brown~~) and Gipuzkoa inventories (red).~~). Landslide distribution map for Spot 2020, GSI Historic, GSI Field and Gipuzkoa inventories. Summary table of the inventories.

	~~Gipuzkoa~~	~~Spot 2020~~	~~GSI Historic~~	~~GSI Field~~
~~Number of landslides~~	~~542~~	~~82~~	~~1240~~	~~25~~
~~Source~~	~~Field survey~~	~~Satellite image photo-interpretation~~	~~Miscellaneous~~	~~Field survey~~
~~Geometry type~~	~~Polygons~~	~~Polygons~~	~~Points and polygons~~	~~Points~~

~~Table~~ 4 Results

4.1~~: Descriptive table for the landslide inventories.~~

~~6~~ Classified Estimated Visibility ~~class maps~~map

We obtained the ~~visibility class maps for field-based inventories in the two~~ EV map of the study ~~areas~~area using r.survey with the settings listed in Tab. ~~2.~~

~~In Gipuzkoa we deployed points every 200 m along the road paths followed during the field-work. According to the experiments carried out in Bornaetxea et al. (2018) 200 m was considered suitable for this concrete case. In Darjeeling we knew that field-based inventories were produced by visual inspection from roads but not the real path followed by the surveyors. As a consequence, we~~1. We used the entire road network (including roads slightly outside the boundaries of the studied area) and a maximum distance between points of 50 m for modelling the ~~visibility.~~estimated visibility of an observer

Con formato: Fuente: 9 pto, Negrita, Color de fuente: Negro

Con formato: Normal, Espacio Después: 10 pto, Borde: Superior: (Sin borde), Inferior: (Sin borde), Izquierda: (Sin borde), Derecha: (Sin borde), Entre : (Sin borde)

Con formato: Fuente: 9 pto, Negrita, Color de fuente: Negro

Con formato: Fuente: 9 pto, Negrita

Con formato: Color de fuente: Negro

Con formato: Título 2

Con formato: Diseño: Claro (Color personalizado(RGB(252;252;252)))

Con formato: Diseño: Claro (Color personalizado(RGB(252;252;252)))

Con formato: Color de fuente: Negro

Con formato: Normal, Borde: Superior: (Sin borde), Inferior: (Sin borde), Izquierda: (Sin borde), Derecha: (Sin borde), Entre : (Sin borde), Punto de tabulación: 7,96 cm, Centrado + 15,92 cm, Derecha

moving along the study area. We considered all the possible roads accessible in the study area, even though this probably overestimates the actual places from which the territory is commonly observed.

~~We set to infinity (Tab. 2)~~The EV map was calculated for hypothetical landslides with an area equal to 78.54 m², which corresponds to the smallest landslides inventoried in Darjeeling (Tab. 1). We set to infinity the maximum line of sight distance in order to assess the visibility level for the complete territory.~~ We calculated maximum solid angle (SA) maps for hypothetical landslides with an area similar to the smallest landslides inventoried in Gipuzkoa and Darjeeling (Tab. 2), and we assumed that larger landslides were therefore visible.~~

	~~**Gipuzkoa**~~	**Darjeeling**
Distance between points	~~200~~	50
Number of points	~~14352~~	11054
Maximum visible distance		infinity ~~infinity~~
DTM resolution (m)	~~5~~	10
Target Object size (m²)	~~19.63~~	78.54

Table ~~2~~1: Summary of the specific settings to calculate *SA* maps for each study area.

We classified the ~~*SA* maps~~EV map in 6 classes ~~(*SAc map*),~~ using 16.67th, 33.33th, 50th, 66.67th, and 83.33th and 100th quantiles, of the SA map values, as thresholds. Then we applied ~~the~~a 3x3 smoothing moving window~~ smoothing~~. Details about the ~~*SAc* maps and the~~ threshold values for each SA class are available in ~~Tab. 3 and~~ Fig. 4.

		~~Gipuzkoa~~		~~Darjeeling~~	
~~Quant.~~	~~Class~~	~~Bin (min²)~~	~~Area (km²)~~	~~Bin (min²)~~	~~Area (km²)~~
~~100.0~~	~~1~~	~~4897.85 – 74141600~~	~~334.93~~	~~4561.02 - 74141601~~	~~90.87~~
~~83.33~~	~~2~~	~~1039.20 – 4897.85~~	~~329.46~~	~~942.98 - 4561.02~~	~~88.124~~
~~66.67~~	~~3~~	~~271.42 – 1039.20~~	~~328.31~~	~~345.36 - 942.98~~	~~85.29~~
~~50.0~~	~~4~~	~~63.27 – 271.42~~	~~328.23~~	~~150.36 - 345.36~~	~~83.27~~
~~33.33~~	~~5~~	~~4.67 – 63.27~~	~~328.18~~	~~59.74 - 150.36~~	~~81.94~~

Celdas eliminadas
Con formato: Fuente: Times New Roman
Con formato: Fuente: Times New Roman, Color de fuente: Automático
Con formato: Fuente: Times New Roman
Tabla con formato
Con formato
Con formato
Con formato: Fuente: Times New Roman
Con formato: Izquierda
Con formato: Fuente: Times New Roman
Con formato
Con formato
Con formato: Izquierda
Con formato: Fuente: Times New Roman
Con formato: Fuente: Times New Roman
Con formato
Con formato
Celdas eliminadas
Con formato: Fuente: Times New Roman
Con formato: Izquierda
Con formato: Fuente: Times New Roman
Celdas eliminadas
Con formato
Con formato
Con formato: Fuente: Times New Roman
Con formato: Izquierda
Con formato: Fuente: Times New Roman
Con formato
Con formato
Con formato: Fuente: Times New Roman
Con formato: Izquierda
Con formato: Fuente: Times New Roman
Con formato: Fuente: 9 pto, Negrita
Con formato: Fuente: 9 pto, Negrita
Con formato: Normal, Espacio Después: 10 pto
Con formato: Fuente: 9 pto, Negrita
Con formato: Color de fuente: Negro
Con formato

~~16.67~~	~~6~~	~~0.0 – 4.67~~	~~326.99~~	~~0 – 59.74~~	~~84.21~~
	~~Total~~		~~1976.12~~		~~513.70~~

~~**Table 3: Details about the visibility classes for Gipuzkoa and Darjeeling study areas. The abbreviation Quant. Refers to quantiles. min² stands for square minutes, a unit of measure of the solid angle.**~~

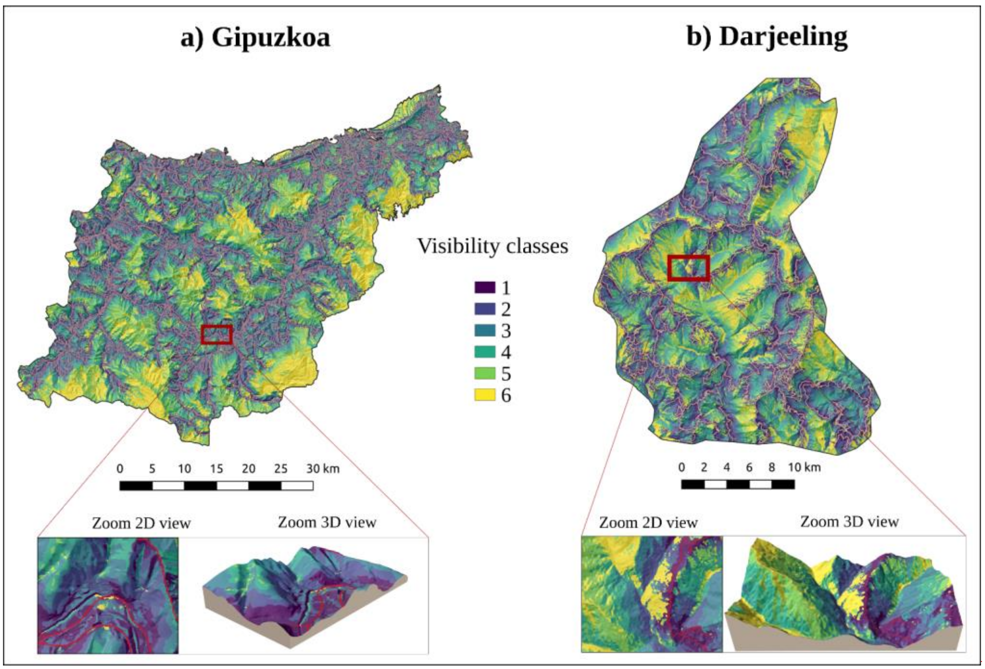

Con formato: Color de fuente: Negro

Con formato: Normal, Borde: Superior: (Sin borde), Inferior: (Sin borde), Izquierda: (Sin borde), Derecha: (Sin borde), Entre : (Sin borde), Punto de tabulación: 7,96 cm, Centrado + 15,92 cm, Derecha

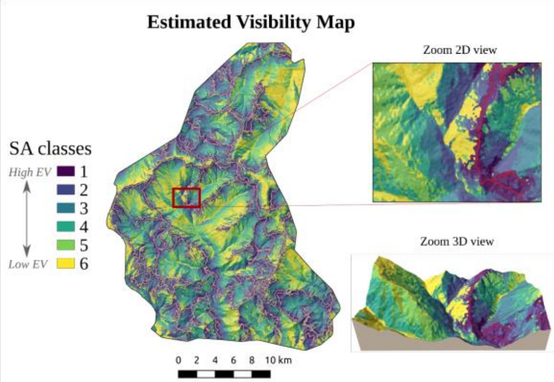

Quant.	SA class	Bin (min²)	Area (km²)
100	1	4561.02 - 74141601	90.87
83.33	2	942.98 - 4561.02	88.124
66.67	3	345.36 - 942.98	85.29
50	4	150.36 - 345.36	83.27
33.33	5	59.74 - 150.36	81.94
16.67	6	0 - 59.74	84.21

Figure 4: ~~Visibility class~~**EV, map for an object having a size of** ~~Gipuzkoa and Darjeeling study areas~~**78.54 m^2. Red lines in the zoom insets represent the roads used as reference observation points. The abbreviation Quant. refers to quantiles and min^2 stands for square minutes, a unit of measure of the solid angle.**

~~The territory~~ We carried out a spatial analysis to investigate possible natural causes for different landslide density in the different ~~visibility~~SA classes ~~is quite homogeneous in terms of morphometry~~(see Fig. 5). Terrain slope, lithology and land use ~~as shown in~~are the ~~plots of (i)~~most important factors that may condition the ~~probability density~~occurrence of landslides (Reichenbach et al. 2018). So, we analysed the empirical densities distribution of the ~~Slope~~slope values and ~~(ii)~~ the percentual spatial coverage of the ~~Lithology and Land Use categories (Fig. 5).~~

~~The slope distribution in Gipuzkoa (Fig. 5a) shows a local maximum for the very low slope values in visibility classes 1, 2 and 3. This is probably due to the fact that roads in Gipuzkoa are mainly on the valley floor, and consequently the plains are located in the most visible portions of the territory. In Darjeeling (Fig. 5b), where roads are primarily located along ridges, slope values are very homogeneous among the visibility classes. Concerning~~ lithology~~, in Gipuzkoa (Fig. 5a) only the slate rocks show a relevant difference in class 6. This is due to the localized outcrop of this metamorphic material in the eastern part of the territory. Regarding the~~ and land ~~use, although the general trends are always homogeneous, anthropic and grass land uses are dominant in the most visible classes (classes 1 and 2), while forests and scrubs and hedges are more abundant in the less visible classes. In Darjeeling (Fig. 5b),~~ cover categories inside each SA class. Figure 5 shows that slope empirical distributions are similar among the SA classes, and so are the distributions of the lithological and land ~~use~~cover categories~~ are also similarly represented within the different visibility classes.~~. Data in Fig. 5 suggests that any difference in landslide density, between SA classes, is unlikely to be related to morphology, land cover, and lithology.

Con formato: Fuente: 9 pto, Negrita
Con formato: Fuente: 9 pto, Negrita
Con formato: Fuente: 9 pto, Negrita
Con formato: Fuente: 9 pto, Negrita
Con formato: Normal, Espacio Después: 10 pto
Con formato: Color de fuente: Negro
Con formato: Normal, Borde: Superior: (Sin borde), Inferior: (Sin borde), Izquierda: (Sin borde), Derecha: (Sin borde), Entre : (Sin borde), Punto de tabulación: 7,96 cm, Centrado + 15,92 cm, Derecha

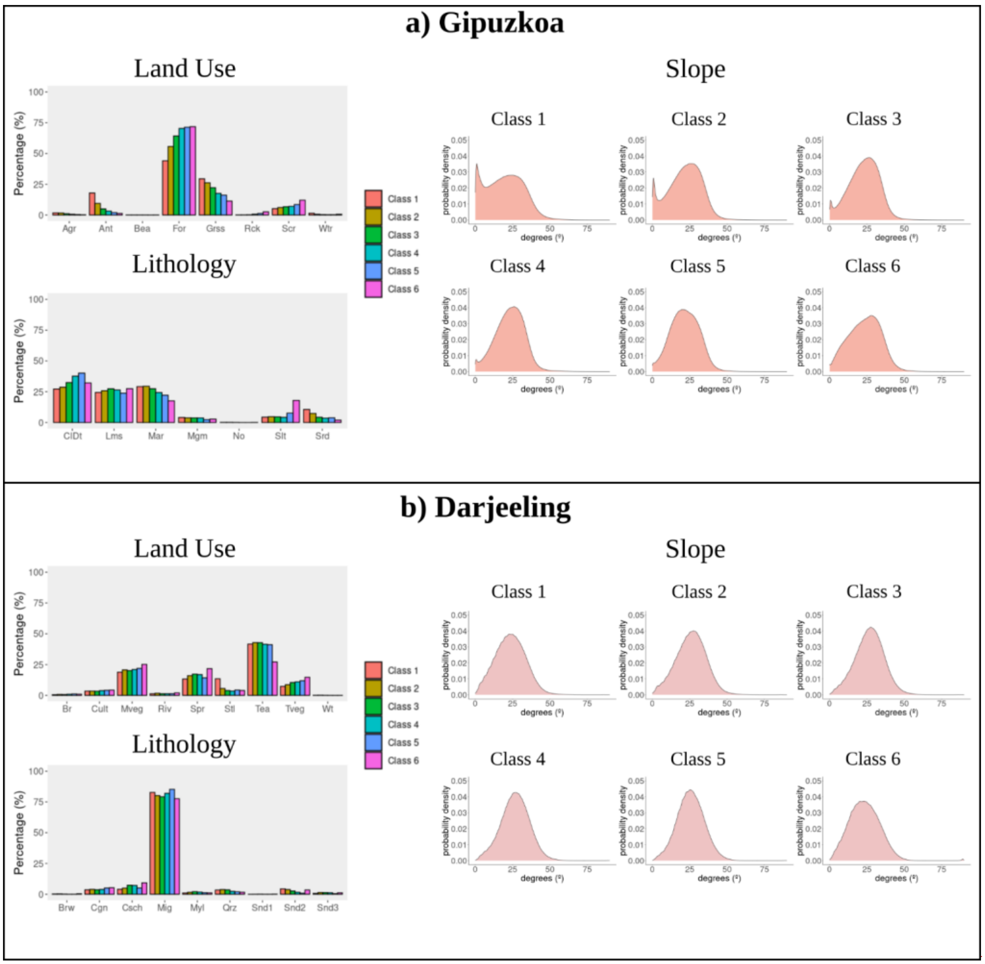

Con formato: Color de fuente: Negro

Con formato: Normal, Borde: Superior: (Sin borde), Inferior: (Sin borde), Izquierda: (Sin borde), Derecha: (Sin borde), Entre : (Sin borde), Punto de tabulación: 7,96 cm, Centrado + 15,92 cm, Derecha

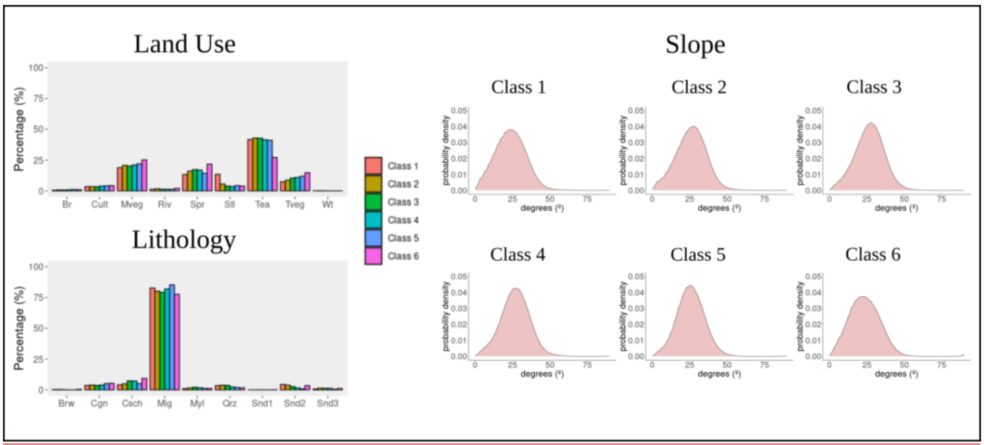

Figure 5: Slope probability density plots and Land Use and Lithology distribution by ~~visibility~~SA classes for ~~Gipuzkoa and Darjeeling study areas. In Gipuzkoa land use types are Agr: Agricultural; Ant: Antropic; Bea: Beach and peatlands; For: Forest; Grss: Grass; Rck: Rock; Scr: Scrub and hedges; Wtr: Water. The Lithology types are ClDt: Clay and Detrital rock; Lms: Limestones; Mgm: Magmatic rocks; Mar: Marls; No: No rock; Slt: Slate; Srd: Surface deposits. In Darjeeling land~~Darjeeling study areas. Land use types are Br: Barren; Cult: Cultivated land; Mveg: Moderate vegetation; Riv: River; Stl: Settlement; Spr: Sparse vegetation; Tea: Tea plantation; Tveg: Thick vegetation; Wt: Waterbody. The lithology types are Mig: Banded migmatite, Gt-Bt gneiss, mica schist, biotite gneiss; Brw: Brownish, yellow oxidised soil with boulders-pebbles and latsol; Cgn: Calc granulite, quartzite, gneiss, Gar, Sil, Kya schists; Csch: Chlorite sericite schist and quartzite, meta-graywacke; Myl: Mylonitic granite gneiss; Qrz: Quartz arenite, black slate, cherty phyllite, quartzite; Snd1: Sand, silt and clay; Snd2: Sandstone, clay, shale, conglomerate; Snd3: Sandstone, shale with minor coal.

~~7~~4.2 Description and analysis of ~~the results~~

~~In Fig. 6 we show~~ NLC ~~values for the Gipuzkoa Inventory, which is a strictly field based landslide database. Figure 6 highlights that the majority of landslides are located in very visible areas i.e., classes 1 to 3, and only a negligible number of landslides is located in scarcely visible areas (class 5 or 6). Data show a near monotonic decrease of the NLC as the level of the visibility decreases, or what is equivalent, as the visibility class increases.~~plots

Figure 6 shows NLC versus the SA classes of the EV map, for the available landslide inventories. Fig. 6a shows that, in the GSI Field inventory (a field-based-inventory), most of the landslides are located within the classes having higher SA values (class 1 and class 2). Landslide density in the other classes is very fluctuating, probably due to the small number of landslides in the inventory.

Con formato: Fuente: 9 pto, Negrita

Con formato: Fuente: 9 pto, Negrita

Con formato: Normal, Espacio Después: 10 pto

Con formato: Fuente: 9 pto, Negrita

Con formato: Título 2

Con formato: Color de fuente: Negro

Con formato: Normal, Borde: Superior: (Sin borde), Inferior: (Sin borde), Izquierda: (Sin borde), Derecha: (Sin borde), Entre : (Sin borde), Punto de tabulación: 7,96 cm, Centrado + 15,92 cm, Derecha

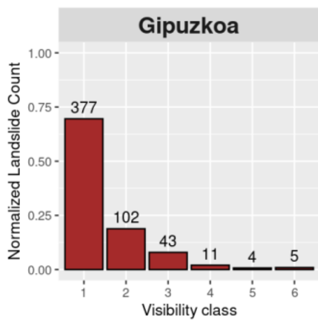

GSI Historic (Fig.

6b) includes landslides mapped using different methods. It shows a slight, but monotonic, decreasing trend.

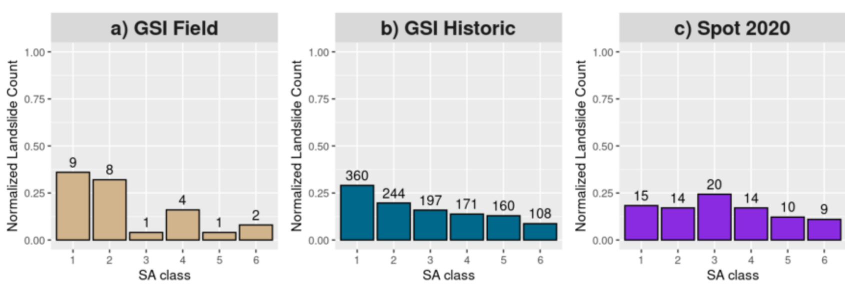

Figure **6**: Normalized landslide count~~ distribution plot for Gipuzkoa inventory. The values above each column indicate the number of landslides in each visibility class.~~

Con formato: Color de fuente: Negro

Con formato: Color de fuente: Negro

Con formato: Color de fuente: Negro

Con formato: Normal, Borde: Superior: (Sin borde), Inferior: (Sin borde), Izquierda: (Sin borde), Derecha: (Sin borde), Entre : (Sin borde), Punto de tabulación: 7,96 cm, Centrado + 15,92 cm, Derecha

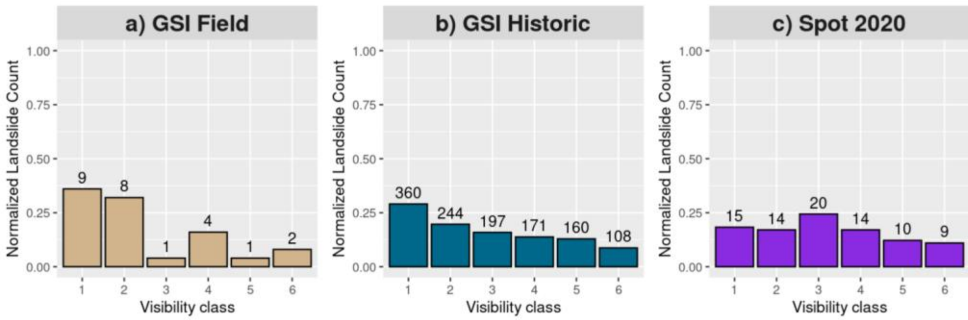

~~Figure 7: Normalized landslide-count distribution~~ **plot for GSI Field, GSI Historic and Spot 2020 inventories. The values above each column signify the number of landslides in each ~~visibility~~SA class.**

Figure ~~7 shows NLC versus visibility classes for the landslide inventories of Darjeeling. In GSI Field (a field-based inventory), we used single points to locate the (few) landslides (Fig. 7a), and we sampled visibility class values from the pixel in which they fell. As expected, most of the landslides are located within the most visible classes (class 1 and class 2). The values in the other classes are very fluctuating but this is probably due to the fact that the number of landslides in the inventory is very small.~~6c

~~GSI Historic (Fig. 7b) includes landslides mapped using different methods and shows a slight, but still monotonic, decreasing trend.~~

~~Figure 7c~~ shows the calculated ~~NLS~~NLC values for the Spot 2020 inventory, produced ~~solely by~~through photo-interpretation of satellite imagery. The values calculated in the ~~visibility~~SA classes are fairly homogeneous and ~~show a non-monotonic trend~~without trends.

GSI Historic inventory contains two main types of information: landslides mapped exploiting satellite/aerial images or collected during field-based survey and from legacy data. We separated data obtained by satellite/aerial images from the rest of the data sources and called them GSI Historic Sat and GSI Historic Others respectively.

NLC values show a pronounced monotonic decreasing trend for the GSI Historic Others inventory (Fig. ~~8a), copying~~7a) while GSI Historic Sat (Fig. 7b) behaves similarly to the ~~pattern observed for the field-based Gipuzkoa~~Spot 2020 inventory (Fig. ~~6).~~ 6c), with the landslide density not dependent on SA classes.

Con formato: Fuente: 9 pto, Negrita, Color de fuente: Negro

Con formato: Normal, Espacio Después: 10 pto, Borde: Superior: (Sin borde), Inferior: (Sin borde), Izquierda: (Sin borde), Derecha: (Sin borde), Entre : (Sin borde)

Con formato: Fuente: 9 pto, Negrita, Color de fuente: Negro

Con formato: Color de fuente: Negro

Con formato: Color de fuente: Negro

Con formato: Normal, Borde: Superior: (Sin borde), Inferior: (Sin borde), Izquierda: (Sin borde), Derecha: (Sin borde), Entre : (Sin borde), Punto de tabulación: 7,96 cm, Centrado + 15,92 cm, Derecha

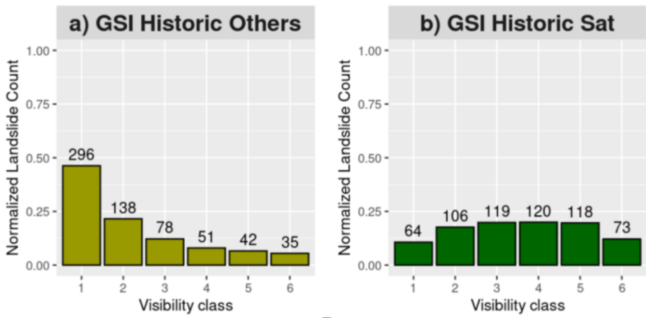

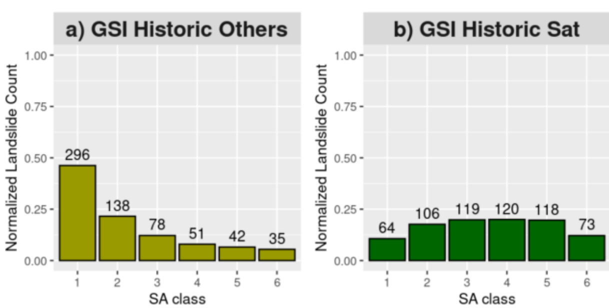

Figure ~~8~~7: Normalized landslide count distribution plot for GSI Historic Others and GSI Historic Sat inventories. The values above each column signify the absolute number of landslides in each visibility class.

~~The GSI Historic Sat (Fig. 8b) shows a similar trend to that observed for the Spot 2020 inventory (Fig. 7c), with the landslide density not dependent on visibility classes.~~

We additionally compared landslides sizes in the different ~~visibility~~SA classes (Fig. ~~9~~8). In ~~Gipuzkoa and~~ GSI Historic Others we merged ~~respectively classes 3,4,5,6 and~~ 4,5,6 to have enough samples. We did not consider Spot 2020 and GSI Field inventories because of the little amount of data.

Con formato: Fuente: 9 pto, Negrita, Color de fuente: Negro

Con formato: Fuente: 9 pto, Negrita, Color de fuente: Negro

Con formato: Normal, Espacio Después: 10 pto, Borde: Superior: (Sin borde), Inferior: (Sin borde), Izquierda: (Sin borde), Derecha: (Sin borde), Entre : (Sin borde)

Con formato: Color de fuente: Negro

Con formato: Diseño: Claro (Color personalizado(RGB(252;252;252)))

Con formato: Color de fuente: Negro

Con formato: Normal, Borde: Superior: (Sin borde), Inferior: (Sin borde), Izquierda: (Sin borde), Derecha: (Sin borde), Entre : (Sin borde), Punto de tabulación: 7,96 cm, Centrado + 15,92 cm, Derecha

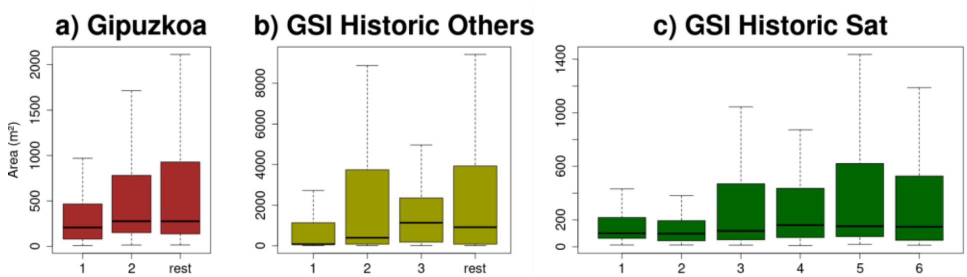

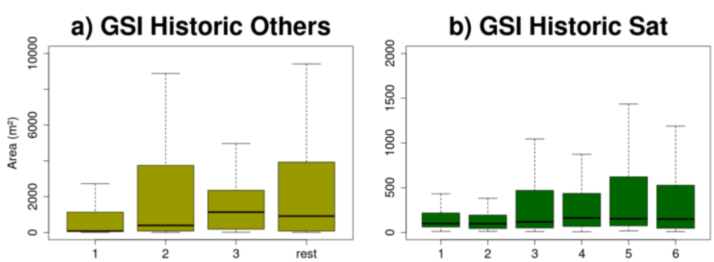

Figure ~~9~~8: Landslide area boxplots per ~~visibility~~SA classes. Numbers in ~~absceises~~the x axis are the ~~visibility~~SA classes of the EV map. Horizontal solid line, inside each box, indicates the median value.

Landslides in class 1 are significantly smaller than those included in the other classes~~,~~ for ~~both Gipuzkoa and~~ GSI Historic Others ~~inventories~~inventory (Fig. ~~9a and 9b~~8a). Furthermore, the landslide size ~~central value in these two inventories~~median in this inventory tends to increase ~~with~~when the ~~decrease of the~~ estimated visibility ~~class, while~~decreases (i.e., the ~~maximum variation~~median of the ~~median~~ landslide area in classes 3,4,5,6 is ~~188%~~up to 20 times larger than in class 1 and ~~2000% respectively.~~2). For the GSI Historic Sat ~~landslide sizes (Fig. 9c)~~ we did not observe a clear increasing trend in the ~~median value,~~medians of the landslide sizes (Fig. 8b) which ~~shows a considerably smaller maximum variation, 66%.~~ are more homogeneous across the SA classes (even if in classes 1 and 2 landslides are generally small).

4.3 Testing the method with external and modelled data

We performed two additional analyses to further confirm the observed behaviour. First, we verified how many of the landslides recorded in Spot 2020 and GSI Historic Sat inventories would have been visible if observed from the same roads used to estimate the visibility for the other inventories. Second, we applied the EV analysis to a purely field-based inventory available for a different study area.

Con formato: Fuente: 9 pto, Negrita, Color de fuente: Negro

Con formato: Fuente: 9 pto, Negrita, Color de fuente: Negro

Con formato: Fuente: 9 pto, Negrita, Color de fuente: Negro

Con formato: Fuente: 9 pto, Negrita

Con formato: Fuente: 9 pto, Negrita, Color de fuente: Negro, Diseño: Claro (Color personalizado(RGB(252;252;252)))

Con formato: Fuente: 9 pto, Negrita, Color de fuente: Negro, Diseño: Claro (Color personalizado(RGB(252;252;252)))

Con formato: Normal, Espacio Después: 10 pto, Borde: Superior: (Sin borde), Inferior: (Sin borde), Izquierda: (Sin borde), Derecha: (Sin borde), Entre : (Sin borde)

Con formato: Fuente: 9 pto, Negrita, Color de fuente: Negro, Diseño: Claro (Color personalizado(RGB(252;252;252)))

Con formato: Diseño: Claro (Color personalizado(RGB(252;252;252)))

Con formato: Diseño: Claro (Color personalizado(RGB(252;252;252)))

Con formato: Diseño: Claro (Color personalizado(RGB(252;252;252)))

Con formato: Diseño: Claro (Color personalizado(RGB(252;252;252)))

Con formato: Diseño: Claro (Color personalizado(RGB(252;252;252)))

Con formato: Diseño: Claro (Color personalizado(RGB(252;252;252)))

Con formato: Diseño: Claro (Color personalizado(RGB(252;252;252)))

Con formato: Diseño: Claro (Color personalizado(RGB(252;252;252)))

Con formato: Diseño: Claro (Color personalizado(RGB(252;252;252)))

Con formato: Diseño: Claro (Color personalizado(RGB(252;252;252)))

Con formato: Diseño: Claro (Color personalizado(RGB(252;252;252)))

Con formato: Diseño: Claro (Color personalizado(RGB(252;252;252)))

Con formato: Color de fuente: Negro

Con formato: Normal, Borde: Superior: (Sin borde), Inferior: (Sin borde), Izquierda: (Sin borde), Derecha: (Sin borde), Entre : (Sin borde), Punto de tabulación: 7,96 cm, Centrado + 15,92 cm, Derecha

For the first analysis we estimated the solid angle of the landslides included in Spot 2020 and GSI Historic Sat inventories (by considering their real size). Then we selected only those landslides with a SA larger than 400 square minutes, which is a value slightly larger than a person's maximum visual acuity (Bornaetxea and Marchesini, 2021; Healey and Sawant, 2012). We refer to these two samples as “Spot 2020 visible” and “GSI Historic Sat visible” respectively. In this scenario, the number of (potentially) visible landslides became 55 for “Spot 2020 visible” and 301 for “GSI Historic Sat visible”, i.e. -59.8% and -32.9% with respect to the original datasets.

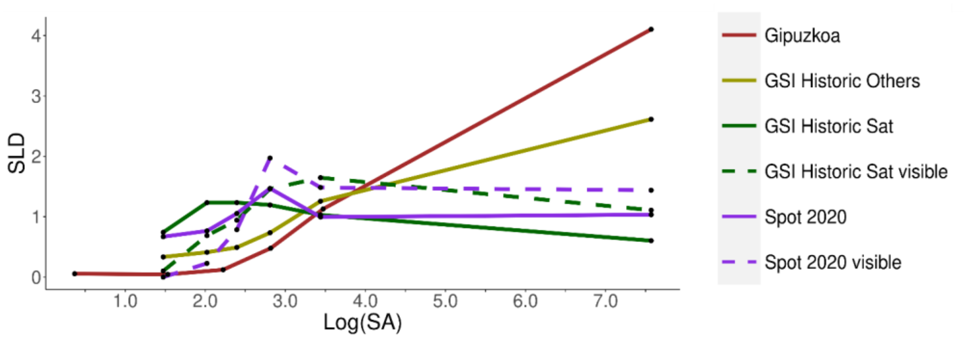

Figure 9: Standardized landslide density plot for six different landslide inventories. Spot 2020 visible and GSI Historic Sat visible are simulated sub samples of Spot 2020 and GSI Historic Sat respectively.

For the second analysis, we used a landslide inventory prepared, by one of the authors, during a field-work campaign carried out in the period from June to August 2016 in Gipuzkoa Province (Spain) (Bornaetxea et al., 2018). The inventory includes 542 shallow landslides. The roads followed during the survey are known. This inventory is referred to as **Gipuzkoa** inventory. ~~also~~We applied the approach explained in section 3, but using a 5x5 meters resolution DTM and a distance of 200 meters between observation points.

Results are shown in Fig. 9, where we compared the standardized landslide density (SLD, see section 3) values with respect to the central value of each ~~visibility~~SA class ~~(Fig. 10), in order to allow a comparable contrast between all the inventories (visibility~~. SA values ~~were~~are plotted in logarithmic scale~~). We~~ and we excluded GSI Field and GSI Historic inventories from this analysis due to data scarcity or because of the non-homogeneous source of the data.

In Fig. ~~In Fig. 10 Gipuzkoa and GSI Historic Others show a monotonically non decreasing behaviour where the amount of landslide increases with the solid angle value, i.e., when the terrain visibility from the roads increases.~~9 we observe that, for values of log(SA) smaller than about 3.0 (where the central value of the SA classes 3, 4, 5 and 6 are), “Spot 2020 visible” and

Con formato: Color de fuente: Negro

Con formato: Normal, Borde: Superior: (Sin borde), Inferior: (Sin borde), Izquierda: (Sin borde), Derecha: (Sin borde), Entre : (Sin borde), Punto de tabulación: 7,96 cm, Centrado + 15,92 cm, Derecha

"GSI Historic Sat visible" show a marked reduction of the SLD respect to the original Spot 2020 and GSI Historic Sat inventories. The reduction is caused by the worse visibility from roads than from satellites in classes from 3 to 6.

In the same range of log(SA) values, the pattern of SLD for the "Spot 2020 visible" and "GSI Historic Sat visible" inventories is monotonically non decreasing, likewise the GSI Historic Others inventory.

From Fig. 9 we note that also the Gipuzkoa inventory, entirely field-based, shows a marked monotonically non decreasing pattern. The SLD curve is similar to GSI Historic Others in shape, which suggests that both show a substantial dependence from the EV. This is also conformal to the pattern of the SLD values for the "Spot 2020 visible" and "GSI Historic Sat visible" inventories when SA is low. In contrast, GSI Historic Sat and Spot 2020 show an almost flat behaviour, where the number of landslides does not vary according to ~~level of visibility~~the EV from the roads.

~~We further simulated the visibility of landslides included in the GSI Historic Sat and Spot 2020 inventories from roads. By setting a visibility threshold of 400 square minutes (which is slightly larger than a person's maximum visual acuity (Bornaetxea and Marchesini, 2021; Healey and Sawant, 2012), we calculated the SLD values for the landslides potentially visible from roads (Fig. 10). In this scenario, the number of (potentially) visible landslides is 55 (-32.9%) and 301 (-59.8%) for **Spot 2020 visible** and **GSI Historic Sat visible** respectively. Furthermore, for values of log(SA) smaller than about 3.5 and 3.0, the graphs of GSI Historic Sat Visible and Spot 2020 Visible respectively show a monotonically increasing pattern. In the simulation, missing landslides are mostly in areas with poor visibility.~~

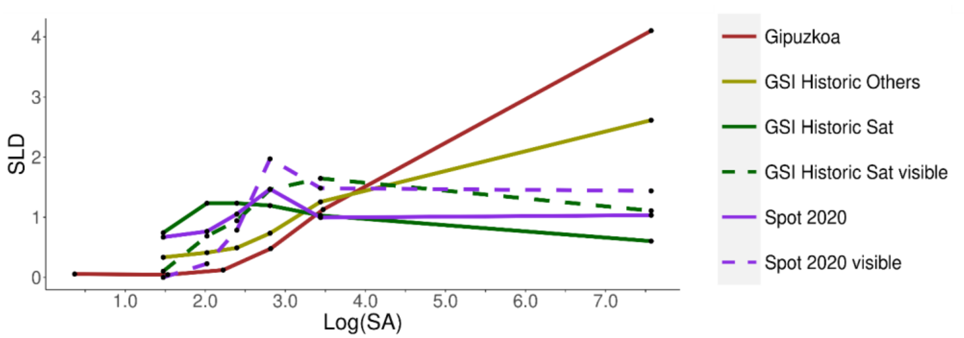

~~**Figure 10: Normalized landslide count distribution plot for GSI Historic Others and GSI Historic Sat inventories. The values above each column signify the absolute number of landslides in each visibility class.**~~

~~**8 Discussion**~~

~~We analysed the~~ It is interesting to note that for the highest log(SA) values (i.e., for estimated visibility class 1), the SLD values for "Spot 2020 visible" and "GSI Historic Sat visible" are similar to those in the original inventories. This shows that the landslides in class 1 can all be mapped from roads.

Con formato: Color de fuente: Negro

Con formato: Normal, Borde: Superior: (Sin borde), Inferior: (Sin borde), Izquierda: (Sin borde), Derecha: (Sin borde), Entre : (Sin borde), Punto de tabulación: 7,96 cm, Centrado + 15,92 cm, Derecha

5 Discussion

In this paper, we assess the CoLM uniformity of landslides inventories in relationship ~~between the terrain visibility and the information on landslides in four inventories prepared with different data and methods. In particular, we contrasted information on the density of landslides collected in the field or~~with the visibility offered by ~~archive data collection with those obtained through photo interpretation of satellite images. For surveys conducted from roads we modelled visibility~~well-known observation points. We estimated the visibility offered by a set of points of observation using a geometric approach ~~taking~~that takes into account the local morphology of ~~the~~a territory. The most visible areas are generally located ~~in~~near the ~~vicinity~~points of observations (i.e. roads~~, with a progression often differing substantially from~~ in this work). But, unlike in the geometric distance buffering~~. This is shown in Fig. 4a (Gipuzkoa) and in Fig. 4b (Darjeeling) by the lack of symmetry of the boundaries of the~~, the SA classes ~~(with respect to roads) and by the presence of~~show a non-symmetric propagation of the EV, which allows to detect portions of territories very close to roads but ~~not~~poorly visible ~~from roads.~~ (Fig. 4).

~~In the field based Gipuzkoa inventory, landslide density correlates positively with terrain visibility, showing a monotonic decreasing trend (Fig. 6). Furthermore, the median size of the landslides is larger in the less visible classes (Fig. 9a).~~

The spatial densities of landslide information (measured by the NLC and SLD metrics) and the estimated visibility ~~classes~~(EV) are positively ~~correlated also in~~related to the GSI Field (Fig. ~~7b~~6a) and GSI Historic Others (Fig. ~~8a~~7a) inventories. The deviations from a monotonic trend, observed in the GSI Field inventory, are probably related to the low data density and location inaccuracy. Since the distribution of the main landslide predisposing factors is homogeneous across all the SA classes (Fig. 5), we consider these trends as relevant evidence of the scarce CoLM uniformity of the inventories and, as a consequence, of their uneven completeness. On the contrary, for the satellite imagery-based inventories (Spot 2020 and GSI Historic Sat) the NLC and SLD values in the SA classes are quite uniform (Fig. 6c and 7b). This is assumed to be a consequence of the neutral CoLM uniformity offered by the remote acquisition.

~~We assert that limited visibility or complete lack of visibility from observation points along the roads hampered the possibility to detect landslides, in particular when small.~~

~~In the inventories based on satellite imagery (Spot 2020 and GSI Historic Others) the density of landslides in the visibility (from roads) classes is quite uniform (Fig. 7c and 8b). Furthermore, for the GSI Historic Sat inventory, the variation of landslide size in the different visibility classes does not show a clear trend and presents much smaller variations than the Gipuzkoa and GSI Historic Others inventories. This is assumed to be a consequence of the neutral observation point offered by the remote acquisition.~~

~~Visibility can explain the lower capacity of field surveyors to detect landslides located in remote areas, and the higher capacity to detect small landslides along the road. On the other hand, landslide mapping through satellite image photo interpretation showed an overall homogeneous performance, mainly because the single observation point offered a constant visibility level along the territory. In this case, limits in the spatial resolution and in the acquisition geometry,~~Roads, which

Con formato: Color de fuente: Negro

Con formato: Normal, Borde: Superior: (Sin borde), Inferior: (Sin borde), Izquierda: (Sin borde), Derecha: (Sin borde), Entre : (Sin borde), Punto de tabulación: 7,96 cm, Centrado + 15,92 cm, Derecha

are by definition always included~~ can be the factors hampering the possibility of mapping small landslides (Mondini et al., 2014).~~

~~The areas covered by each visibility class are similar in terms of landslide predisposing factors such as morphometry, lithology and land use (Fig. 5). Roads, present only~~ in the first visibility class, are also considered by many authors as a predisposing factor since cut-and-fill failures, drainage and groundwater alteration can influence the occurrence of landslides (Brenning et al., 2015; Donnini et al., 2017; Giordan et al., 2018; McAdoo et al., 2018~~; ~~). Moreover, Taylor et al. (2020) suggest that transport networks and landslides are interconnected in terms of process and impacts. Indeed, Tanyaş et al. (2022) also state that road construction acts as a major causative factor of landslides. However, the reasons of that close relationship are very complex and not fully unravelled (Meneses et al., 2019; Santangelo et al., 2015; Sidle et al., 2014; Sidle and Ziegler, 2012~~). ~~), which justifies the need to investigate whether the major availability of roadside landslide information in inventories may also depend on other factors.

Based on the above considerations, a higher density of landslides (higher NLC and SLD values) should be expected ~~in~~ only along the roads and, as a consequence, in the SA class 1 ~~than in~~respect to the SA classes 2 to 6~~, with the latter characterised by~~. But at the same time, all the SA classes but the first one, should show fairly similar density ~~values. This was not observed in~~of landslides. In inventories based on satellite imagery ~~nor~~(GSI Historic Sat and Spot 2020) the latter condition was fulfilled, but we didn't observe a higher number of landslides in ~~those acquired~~SA class 1 (Figs. 6c and 7b). In the GSI Field and GSI Historic Others, the abundance in ~~the field. In~~SA class 1 is evident, but the number of landslides still drops monotonically also in SA classes 2 to 6. So, we conclude that in both types of inventories, there is a data collection effect~~,~~ (Steiger et al. 2021), albeit different.

In fact, since roadside landslides are typically small (Voumard et al., 2018), they can be easily under-represented when the inventories are prepared with images without an adequate resolution or unsuitable acquisition geometry (Martha et al., 2021). ~~On the contrary, when~~When considering ~~inventories based on field surveys and historical data collection (Gipuzkoa, GSI Field and~~ GSI Historic Others~~), small~~, landslides are very abundant in the highly visible areas~~,~~ (Fig. 7a), and ~~very few landslides~~at the same time they are ~~intercepted~~considerably smaller than in the rest of the classes (Fig. 8a). On the contrary, for GSI Historic Sat inventory, comparing Fig. 7b and 8b, we observe a relatively low number of small size landslides in class 1. In this case, limits in the type and quality of the satellite images (e.g., spatial resolution, acquisition time and geometry, etc.), can be the factors hampering the possibility of mapping small landslides (Mondini et al., 2014). ~~low visible areas.~~Furthermore, in GSI Historic Sat the variation of landslide size in the different visibility classes does not show a clear trend and presents much smaller variations than in GSI Historic Others inventories (Fig. 8), where the size of the mapped landslides rises progressively according to the lack of the visibility. This suggests that the visibility can also affect the ~~spatial (Fig. 6, 7a,b) and the size (Fig. 9)~~size distributions (Fig. 8) of the reported landslide information. These results are in line with Steger et al (2021) hypothesis on the "data collection effect", which ~~assumes~~states that the method used to compile inventories can influence the~~ spatial~~ distribution of landslides information in the inventories.

Con formato: Diseño: Claro (Color personalizado(RGB(252;252;252)))

Con formato: Color de fuente: Negro

Con formato: Normal, Borde: Superior: (Sin borde), Inferior: (Sin borde), Izquierda: (Sin borde), Derecha: (Sin borde), Entre : (Sin borde), Punto de tabulación: 7,96 cm, Centrado + 15,92 cm, Derecha

We partially observed a ~~partial~~ monotonic behaviour of the relationship between estimated visibility and landslide density obtained in the field and historic-based inventories also in Spot 2020 Visible and GSI Historic Sat Visible. These two inventories include only those landslides present in the remotely sensed inventories that would result visible through hypothetical field surveys along the roads. SLD values (Fig. ~~10~~9) highlight that the least visible areas (low SA values) lost the majority of landslides. ~~The simulation confirms that the abundance of landslides observed in the most visible areas (high SA values), in inventories prepared by field survey and/or legacy data, was not achieved by the remote sensing-based inventory.~~ ~~Indeed~~Moreover, in the most visible areas, SLD values from the Spot 2020 Visible and GSI Historic Sat Visible inventories are ~~consistently~~ much lower than those observed for the GSI Historic Others ~~and Gipuzkoa inventories.~~. This possibly suggests ~~a possible lack of~~ that some small landslides were not detected in visibility class 1 for Spot 2020 and GSI Historic Sat, eventually caused by the inadequate resolution of the images. ~~Thus, also~~We conclude that even if the CoLM uniformity of the landslide inventories ~~prepared~~produced using ~~inadequate~~ satellite-based images ~~may~~is generally large, they can still be ~~affected by~~ not able to reach, in the SA class 1 (i.e. in the ~~"data collection effect".~~ areas very visible from the roads) the same completeness they have in the other SA classes.

~~Our~~The monotonic non-decreasing trend observed for field–based or legacy-based landslides inventories was confirmed by the analysis carried out with a landslide inventory prepared in a completely different study area, in Spain (Gipuzkoa). For this inventory, the accurate road path followed by the surveyor was also well known and there was not the need to conservatively assess the EV along the entire road network (as we did for the Darjeeling study area). This allowed a more accurate simulation of the EV which, in turn, determined a pronounced non-descending monotonic pattern of the SLD values (Fig. 9). Results obtained on Gipuzkoa confirm that by means of the EV analysis it is possible to assess the CoLM uniformity of an inventory, and therefore also of its completeness. In addition, the use of the SLD metric makes it possible to compare the CoLM uniformity of different inventories produced in the same or in different study areas.

Notwithstanding, we acknowledge that our results depend on some user-driven decisions, such as the distance between observation points placed along the roads, and the choice of the thresholds to obtain the visibility classes. In Darjeeling, the real path followed by the field surveyor ~~is~~was unknown and we applied a conservative approach (visibility overestimation) by considering all roads as potential observation points and a four-time smaller maximum distance between points than in Gipuzkoa. This is probably one of the reasons for the more pronounced monotonic pattern shown in Gipuzkoa with respect to GSI Historic Others. Furthermore, we chose quantile values of the ~~SA~~EV map to obtain ~~visibility~~the SA classes covering similar portions of the study area. We run several tests with different threshold values showing results in terms of landslide densities always very similar to those described by Figs. 6, 7, ~~8, 9,~~ and ~~10~~9.

The resolution of the DTM can also have an impact on the results. A coarse representation of the morphology of the territory can affect the calculation of the solid angle and the delineation of non-visible areas. In this work, we performed the analysis with the higher resolution DTMs available in each study area, but~~,~~ further tests on the influence of the quality of the data should be conducted. Future works should also incorporate the role of the vegetation in the visibility for landslide detection by field-work, although the information about the elevation of each type of vegetation is rare.

Con formato: Color de fuente: Negro

Con formato: Normal, Borde: Superior: (Sin borde), Inferior: (Sin borde), Izquierda: (Sin borde), Derecha: (Sin borde), Entre : (Sin borde), Punto de tabulación: 7,96 cm, Centrado + 15,92 cm, Derecha

~~We think that the procedure and methods presented in this work can be used to: (i) test whether the spatial distribution of landslides in existing inventories (especially those created by fieldwork) is affected by a marked correlation with visibility from observation points, (ii) identify portions of land where landslide density information is enough accurate to calibrate susceptibility, hazard and risk models with more robust data, (iii) identify portions of land where landslide inventories need improvement, (iv) plan exhaustive field mapping campaigns.~~

In addition, although EV could be measured using different metrics (e.g. by counting the number of points that have a direct line of sight to a particular object (Fontani 2017)), we maintain that our method offers the unique perspective of considering several geometric aspects of the object and the territory under investigation. This makes our approach adequate for morphologically complex areas.

6 Conclusions

We analysed the relationship between the spatial density of landslides reported in different inventories prepared through field surveys, collection of previous data and interpretation of remotely acquired images, and the visibility of the territory from observation points located along the roads. We also introduced the concept of uniformity in capacity of landslide mapping (CoLM), as a tool to discern whether the completeness of a landslide inventory is homogeneous across the territory.

The results of the present work show that in inventories prepared using field survey and/or historic legacy data, the ~~spatial distribution of landslides can be strongly affected by the "data collection effect".~~CoLM uniformity can be poor and this is reflected in marked inhomogeneity in completeness. This is demonstrated by (i) the positive correlation observed between landslide density and the visibility of the terrain from the observation points, (ii) the lack of small landslides in areas with low visibility, and (iii) a number of landslides in remote areas intercepted by the satellite images but invisible from roads.

In addition, we observed that inventories based on the use of remote sensing images, ~~can~~where the CoLM is uniform, may also be affected by a different form of "data collection effect~~".~~" (sensu Steiger et al. 2021). In fact, results show that, contrary to what expected (Brenning et al., 2015; Donnini et al., 2017; Giordan et al., 2018; McAdoo et al., 2018; Meneses et al., 2019; Santangelo et al., 2015; Sidle et al., 2014; Sidle and Ziegler, 2012), our inventories don't show abundance of landslides close to roads. Reasons may be searched in the inadequate spatial resolution of the satellite images, that can prevent the recognition of small roadsides landslides.

Thus, our inventories proved not to be uniformly representative of the real spatial distribution of landslides in the study area, requiring for an informed and appropriate usage (Bornaetxea et al., 2018; Steger et al., 2021).

Our procedure enriches the portfolio of solutions to evaluate the quality of landslide inventories introducing local morphology in the analysis. We think that the procedure and methods presented in this work can be used, in other study areas, to: (i) test whether the information in existing inventories (especially those created by fieldwork) is affected by a scarce CoLM (and therefore completeness) uniformity, (ii) identify portions of land where landslide density information is larger with respect to

Con formato: Color de fuente: Negro

Con formato: Normal, Borde: Superior: (Sin borde), Inferior: (Sin borde), Izquierda: (Sin borde), Derecha: (Sin borde), Entre : (Sin borde), Punto de tabulación: 7,96 cm, Centrado + 15,92 cm, Derecha

other areas and can be more properly used to train susceptibility, hazard and risk models, (iii) identify portions of land where landslide inventories need improvement, (iv) plan exhaustive field mapping campaigns.

Data availability

The digital elevation model of Gipuzkoa Province with 5 × 5 meters of resolution, was downloaded from the official geospatial data repository ~~www.geo.euskadi.eus.~~www.geo.euskadi.eus. The Gipuzkoa inventory and the field work paths are data generated by the authors and are available under request. The digital elevation model of Darjeeling with 10 × 10 meters resolution, roads map of Darjeeling and all the landslide inventories used in this work were provided by the Geological Survey of India. The tool r.survey is available in ~~https://doi.org/10.5281/zenodo.3993140.~~https://doi.org/10.5281/zenodo.3993140.

Author contribution

TB and IM conceptualized the work and designed the overall methodology. TB carried out the analysis with the technical assistance of IM and AM. SK and RK provided the necessary data and contributed to interpret the results through their local perspective. TB prepared the first version of the manuscript and IM and AM contributed enormously to its revision and edition. AM coordinated the work and obtained the necessary funds.

Competing interests

The authors declare that they have no conflict of interest.

Acknowledgments

The work was partially funded by the UKRI Natural Environment Research Council's and UK Government's Department for International Development's Science for Humanitarian Emergencies and Resilience research programme (grant number NERC/DFID NE/P000649/1). Txomin Bornaetxea was financially supported by the postdoctoral fellowship program of the Basque Government (grant numbers POS_2020_2_0010) in the framework of a scientific collaboration with the Geological Survey of Canada and during the scientific collaborations with the Geomorphological Group of the Research Institute for the Geo-Hydrological Protection in Perugia, Italian National Research Council (CNR-IRPI).

References

~~Bera, S., Guru, B., and V, R.: Evaluation of landslide susceptibility models: A comparative study on the part of Western Ghat Region, India, Remote Sens. Appl. Soc. Environ., 13, 39–52, https://doi.org/10.1016/j.rsase.2018.10.010, 2019.~~

Con formato: Color de fuente: Negro

Con formato: Normal, Borde: Superior: (Sin borde), Inferior: (Sin borde), Izquierda: (Sin borde), Derecha: (Sin borde), Entre : (Sin borde), Punto de tabulación: 7,96 cm, Centrado + 15,92 cm, Derecha

~~Bornaetxea, T.: Methodological Approach for landslide analysis in a regional scale. Data collection, susceptibility models and precipitation thresholds. Application in Gipuzkoa province (Basque Country), University of the Basque Country (UPV/EHU), Vitoria-Gasteiz, 227 pp., 2018.~~

~~Bornaetxea, T. and Marchesini, I.: r.survey: a tool for calculating visibility of variable-size objects based on orientation, Int. J. Geogr. Inf. Sci., 0, 1–24, https://doi.org/10.1080/13658816.2021.1942476, 2021.~~

~~Bornaetxea, T., Rossi, M., Marchesini, I., and Alvioli, M.: Effective surveyed area and its role in statistical landslide susceptibility assessments, Nat. Hazards Earth Syst. Sci., 18, 2455–2469, https://doi.org/10.5194/nhess-18-2455-2018, 2018.~~

~~Brardinoni, F., Slaymaker, O., and Hassan, M. A.: Landslide inventory in a rugged forested watershed: a comparison between air-photo and field survey data, Geomorphology, 54, 179–196, https://doi.org/10.1016/S0169-555X(02)00355-0, 2003.~~

~~Brenning, A., Schwinn, M., Ruiz-Páez, A. P., and Muenchow, J.: Landslide susceptibility near highways is increased by 1 order of magnitude in the Andes of southern Ecuador, Loja province, Nat. Hazards Earth Syst. Sci., 15, 45–57, https://doi.org/10.5194/nhess-15-45-2015, 2015a.~~

~~Brenning, A., Schwinn, M., Ruiz-Páez, A. P., and Muenchow, J.: Landslide susceptibility near highways is increased by 1 order of magnitude in the Andes of southern Ecuador, Loja province, Nat. Hazards Earth Syst. Sci., 15, 45–57, https://doi.org/10.5194/nhess-15-45-2015, 2015b.~~

~~Cascini, L.: Applicability of landslide susceptibility and hazard zoning at different scales, Eng. Geol., 102, 164–177, https://doi.org/10.1016/j.enggeo.2008.03.016, 2008.~~

~~Chaparro-Cordón, J. L., Rodriguez, E. A., Florez, M. S. R., García-Delgado, H., and Enif Medina Bello: Statistical description of some landslide inventories from Colombian Andes: study cases in Mocoa, Villavicencio, Popayán, and Cajamarca, https://doi.org/10.13140/RG.2.2.17237.04327, 2020.~~

~~Corominas, J., van Westen, C., Frattini, P., Cascini, L., Malet, J.-P., Fotopoulou, S., Catani, F., Van Den Eeckhaut, M., Mavrouli, O., Agliardi, F., Pitilakis, K., Winter, M. G., Pastor, M., Ferlisi, S., Tofani, V., Hervás, J., and Smith, J. T.: Recommendations for the quantitative analysis of landslide risk, Bull. Eng. Geol. Environ., 73, 209–263, https://doi.org/10.1007/s10064-013-0538-8, 2014.~~

~~Cova, T. J., Tsou Ming-Hsiang, Bareth Georg, Song Chunqiao, Song Yan, Cao Kai, and Silva Elisabete A: Comprehensive Geographic Information Systems, Elsevier, 2018.~~

~~Domingo-Santos, J. M., de Villarán, R. F., Rapp-Arrarás, Í., and de Provens, E. C.-P.: The visual exposure in forest and rural landscapes: An algorithm and a GIS tool, Landsc. Urban Plan., 101, 52–58, https://doi.org/10.1016/j.landurbplan.2010.11.018, 2011.~~

~~Donnini, M., Napolitano, E., Salvati, P., Ardizzone, F., Bucci, F., Fiorucci, F., Santangelo, M., Cardinali, M., and Guzzetti, F.: Impact of event landslides on road networks: a statistical analysis of two Italian case studies, Landslides, 14, 1521–1535, https://doi.org/10.1007/s10346-017-0829-4, 2017.~~

Con formato: Color de fuente: Negro

Con formato: Normal, Borde: Superior: (Sin borde), Inferior: (Sin borde), Izquierda: (Sin borde), Derecha: (Sin borde), Entre : (Sin borde), Punto de tabulación: 7,96 cm, Centrado + 15,92 cm, Derecha

~~Fell, R., Corominas, J., Bonnard, C., Cascini, L., Leroi, E., and Savage, W. Z.: Guidelines for landslide susceptibility, hazard and risk zoning for land-use planning, Eng. Geol., 102, 99–111, https://doi.org/10.1016/j.enggeo.2008.03.014, 2008.~~

~~Fiorucci, F., Giordan, D., Santangelo, M., Dutto, F., Rossi, M., and Guzzetti, F.: Criteria for the optimal selection of remote sensing optical images to map event landslides, Nat. Hazards Earth Syst. Sci., 18, 405–417, https://doi.org/10.5194/nhess-18-405-2018, 2018.~~

~~Fressard, M., Thiery, Y., and Maquaire, O.: Which data for quantitative landslide susceptibility mapping at operational scale? Case study of the Pays d'Auge plateau hillslopes (Normandy, France), Nat. Hazards Earth Syst. Sci., 14, 569–588, https://doi.org/10.5194/nhess-14-569-2014, 2014.~~

~~Galli, M., Ardizzone, F., Cardinali, M., Guzzetti, F., and Reichenbach, P.: Comparing landslide inventory maps, Geomorphology, 94, 268–289, https://doi.org/10.1016/j.geomorph.2006.09.023, 2008.~~

~~Gariano, S. L. and Guzzetti, F.: Landslides in a changing climate, Earth-Sci. Rev., 162, 227–252, https://doi.org/10.1016/j.earscirev.2016.08.011, 2016.~~

~~Ghorbanzadeh, O., Meena, S. R., Blaschke, T., and Aryal, J.: UAV-Based Slope Failure Detection Using Deep-Learning Convolutional Neural Networks, Remote Sens., 11, 2046, https://doi.org/10.3390/rs11172046, 2019.~~

~~Giordan, D., Hayakawa, Y., Nex, F., Remondino, F., and Tarolli, P.: Review article: the use of remotely piloted aircraft systems (RPASs) for natural hazards monitoring and management, Nat. Hazards Earth Syst. Sci., 18, 1079–1096, https://doi.org/10.5194/nhess-18-1079-2018, 2018.~~

~~Guzzetti, F., Cardinali, M., and Reichenbach, P.: The AVI project: a bibliographical and archive inventory of landslides and floods in Italy, Environ. Manage., 18, 623–633, 1994.~~

~~Guzzetti, F., Carrara, A., Cardinali, M., and Reichenbach, P.: Landslide hazard evaluation: a review of current techniques and their application in a multi-scale study, Central Italy, Geomorphology, 31, 181–216, https://doi.org/10.1016/S0169-555X(99)00078-1, 1999.~~

~~Guzzetti, F., Reichenbach, P., Ardizzone, F., Cardinali, M., and Galli, M.: Estimating the quality of landslide susceptibility models, Geomorphology, 81, 166–184, https://doi.org/10.1016/j.geomorph.2006.04.007, 2006.~~

~~Guzzetti, F., Mondini, A. C., Cardinali, M., Fiorucci, F., Santangelo, M., and Chang, K.-T.: Landslide inventory maps: New tools for an old problem, Earth-Sci. Rev., 112, 42–66, https://doi.org/10.1016/j.earscirev.2012.02.001, 2012.~~

~~Hao, L., Rajaneesh A, van Westen, C., Sajinkumar K. S, Martha, T. R., Jaiswal, P., and McAdoo, B. G.: Constructing a complete landslide inventory dataset for the 2018 monsoon disaster in Kerala, India, for land use change analysis, Earth Syst. Sci. Data, 12, 2899–2918, https://doi.org/10.5194/essd-12-2899-2020, 2020.~~

~~Healey, C. G. and Sawant, A. P.: On the limits of resolution and visual angle in visualization, ACM Trans. Appl. Percept., 9, 20:1-20:21, https://doi.org/10.1145/2355598.2355603, 2012.~~

~~Hussain, G., Singh, Y., Singh, K., and Bhat, G. M.: Landslide susceptibility mapping along national highway-1 in Jammu and Kashmir State (India), Innov. Infrastruct. Solut., 4, 59, https://doi.org/10.1007/s41062-019-0245-9, 2019.~~

Con formato: Color de fuente: Negro

Con formato: Normal, Borde: Superior: (Sin borde), Inferior: (Sin borde), Izquierda: (Sin borde), Derecha: (Sin borde), Entre : (Sin borde), Punto de tabulación: 7,96 cm, Centrado + 15,92 cm, Derecha

~~Ibsen, M.-L. and Brunsden, D.: The nature, use and problems of historical archives for the temporal occurrence of landslides, with specific reference to the south coast of Britain, Ventnor, Isle of Wight, Geomorphology, 15, 241–258, https://doi.org/10.1016/0169-555X(95)00073-E, 1996.~~

~~Jacobs, L., Dewitte, O., Poesen, J., Maes, J., Mertens, K., Sekajugo, J., and Kervyn, M.: Landslide characteristics and spatial distribution in the Rwenzori Mountains, Uganda, J. Afr. Earth Sci., 134, 917–930, https://doi.org/10.1016/j.jafrearsci.2016.05.013, 2017.~~

~~Jacobs, L., Kervyn, M., Reichenbach, P., Rossi, M., Marchesini, I., Alvioli, M., and Dewitte, O.: Regional susceptibility assessments with heterogeneous landslide information: Slope unit- vs. pixel-based approach, Geomorphology, 356, 107084, https://doi.org/10.1016/j.geomorph.2020.107084, 2020.~~

~~Knevels, R., Petschko, H., Proske, H., Leopold, P., Maraun, D., and Brenning, A.: Event-Based Landslide Modeling in the Styrian Basin, Austria: Accounting for Time-Varying Rainfall and Land Cover, Geosciences, 10, 217, https://doi.org/10.3390/geosciences10060217, 2020a.~~

~~Knevels, R., Petschko, H., Proske, H., Leopold, P., Maraun, D., and Brenning, A.: Event-Based Landslide Modeling in the Styrian Basin, Austria: Accounting for Time-Varying Rainfall and Land Cover, Geosciences, 10, 217, https://doi.org/10.3390/geosciences10060217, 2020b.~~

~~Lee, S., Jang, J., Kim, Y., Cho, N., and Lee, M.-J.: Susceptibility Analysis of the Mt. Umyeon Landslide Area Using a Physical Slope Model and Probabilistic Method, Remote Sens., 12, 2663, https://doi.org/10.3390/rs12162663, 2020.~~

~~Malamud, B. D., Turcotte, D. L., Guzzetti, F., and Reichenbach, P.: Landslide inventories and their statistical properties, Earth Surf. Process. Landf., 29, 687–711, https://doi.org/10.1002/esp.1064, 2004a.~~

~~Malamud, B. D., Turcotte, D. L., Guzzetti, F., and Reichenbach, P.: Landslide inventories and their statistical properties, Earth Surf. Process. Landf., 29, 687–711, https://doi.org/10.1002/esp.1064, 2004b.~~

~~Martha, T. R., Roy, P., Jain, N., Khanna, K., Mrinalni, K., Kumar, K. V., and Rao, P. V. N.: Geospatial landslide inventory of India—an insight into occurrence and exposure on a national scale, Landslides, 18, 2125–2141, https://doi.org/10.1007/s10346-021-01645-1, 2021.~~

~~McAdoo, B. G., Quak, M., Gnyawali, K. R., Adhikari, B. R., Devkota, S., Rajbhandari, P. L., and Sudmeier-Rieux, K.: Roads and landslides in Nepal: how development affects environmental risk, Nat. Hazards Earth Syst. Sci., 18, 3203–3210, https://doi.org/10.5194/nhess-18-3203-2018, 2018.~~

~~Meena, S. R., Mishra, B. K., and Tavakkoli Piralilou, S.: A Hybrid Spatial Multi-Criteria Evaluation Method for Mapping Landslide Susceptible Areas in Kullu Valley, Himalayas, Geosciences, 9, 156, https://doi.org/10.3390/geosciences9040156, 2019.~~

~~Melzner, S., Rossi, M., and Guzzetti, F.: Impact of mapping strategies on rockfall frequency-size distributions, Eng. Geol., 272, 105639, https://doi.org/10.1016/j.enggeo.2020.105639, 2020.~~

~~Meneses, B. M., Pereira, S., and Reis, E.: Effects of different land use and land cover data on the landslide susceptibility zonation of road networks, Nat. Hazards Earth Syst. Sci., 19, 471–487, https://doi.org/10.5194/nhess-19-471-2019, 2019.~~

Con formato: Color de fuente: Negro

Con formato: Normal, Borde: Superior: (Sin borde), Inferior: (Sin borde), Izquierda: (Sin borde), Derecha: (Sin borde), Entre : (Sin borde), Punto de tabulación: 7,96 cm, Centrado + 15,92 cm, Derecha

~~Mondini, A. C., Viero, A., Cavalli, M., Marchi, L., Herrera, G., and Guzzetti, F.: Comparison of event landslide inventories: the Pogliaschina catchment test case, Italy, Nat. Hazards Earth Syst. Sci., 14, 1749–1759, https://doi.org/10.5194/nhess-14-1749-2014, 2014a.~~

~~Mondini, A. C., Viero, A., Cavalli, M., Marchi, L., Herrera, G., and Guzzetti, F.: Comparison of event landslide inventories: the Pogliaschina catchment test case, Italy, Nat. Hazards Earth Syst. Sci., 14, 1749–1759, https://doi.org/10.5194/nhess-14-1749-2014, 2014b.~~

~~Nicu, I. C., Lombardo, L., and Rubensdotter, L.: Preliminary assessment of thaw slump hazard to Arctic cultural heritage in Nordenskiöld Land, Svalbard, Landslides, 18, 2935–2947, https://doi.org/10.1007/s10346-021-01684-8, 2021.~~

~~Park, J.-Y., Lee, S.-R., Lee, D.-H., Kim, Y.-T., and Lee, J.-S.: A regional-scale landslide early warning methodology applying statistical and physically based approaches in sequence, Eng. Geol., 260, 105193, https://doi.org/10.1016/j.enggeo.2019.105193, 2019.~~

~~Piacentini, D., Troiani, F., Daniele, G., and Pizziolo, M.: Historical geospatial database for landslide analysis: the Catalogue of Landslide OCcurrences in the Emilia-Romagna Region (CLOCkER), Landslides, 15, 811–822, https://doi.org/10.1007/s10346-018-0962-8, 2018.~~

~~Reichenbach, P., Rossi, M., Malamud, B. D., Mihir, M., and Guzzetti, F.: A review of statistically-based landslide susceptibility models, Earth-Sci. Rev., 180, 60–91, https://doi.org/10.1016/j.earscirev.2018.03.001, 2018.~~

~~Roberts, S., Jones, J. N., and Boulton, S. J.: Characteristics of landslide path dependency revealed through multiple resolution landslide inventories in the Nepal Himalaya, Geomorphology, 390, 107868, https://doi.org/10.1016/j.geomorph.2021.107868, 2021.~~

~~Rohan, T. and Shelef, E.: Analysis of 311 based Landslide Inventories for Landslide Susceptibility Mapping, AGU Fall Meet. Abstr., 33, 2019.~~

~~Santangelo, M., Marchesini, I., Bucci, F., Cardinali, M., Fiorucci, F., and Guzzetti, F.: An approach to reduce mapping errors in the production of landslide inventory maps, Nat. Hazards Earth Syst. Sci., 15, 2111–2126, https://doi.org/10.5194/nhess-15-2111-2015, 2015.~~

~~Sidle, R. C. and Ziegler, A. D.: The dilemma of mountain roads, Nat. Geosci., 5, 437–438, https://doi.org/10.1038/ngeo1512, 2012.~~

~~Sidle, R. C., Ghestem, M., and Stokes, A.: Epic landslide erosion from mountain roads in Yunnan, China – challenges for sustainable development, Nat. Hazards Earth Syst. Sci., 14, 3093–3104, https://doi.org/10.5194/nhess-14-3093-2014, 2014.~~

~~Stark, C. P. and Hovius, N.: The characterization of landslide size distributions, Geophys. Res. Lett., 28, 1091–1094, https://doi.org/10.1029/2000GL008527, 2001.~~

~~Steger, S., Brenning, A., Bell, R., Petschko, H., and Glade, T.: Exploring discrepancies between quantitative validation results and the geomorphic plausibility of statistical landslide susceptibility maps, Geomorphology, 262, 8–23, https://doi.org/10.1016/j.geomorph.2016.03.015, 2016a.~~

Con formato: Color de fuente: Negro

Con formato: Normal, Borde: Superior: (Sin borde), Inferior: (Sin borde), Izquierda: (Sin borde), Derecha: (Sin borde), Entre : (Sin borde), Punto de tabulación: 7,96 cm, Centrado + 15,92 cm, Derecha

~~Steger, S., Brenning, A., Bell, R., and Glade, T.: The propagation of inventory-based positional errors into statistical landslide susceptibility models, Nat. Hazards Earth Syst. Sci., 16, 2729–2745, https://doi.org/10.5194/nhess-16-2729-2016, 2016b.~~

~~Steger, S., Brenning, A., Bell, R., and Glade, T.: The influence of systematically incomplete shallow landslide inventories on statistical susceptibility models and suggestions for improvements, Landslides, 14, 1767–1781, https://doi.org/10.1007/s10346-017-0820-0, 2017a.~~

~~Steger, S., Brenning, A., Bell, R., and Glade, T.: The influence of systematically incomplete shallow landslide inventories on statistical susceptibility models and suggestions for improvements, Landslides, 14, 1767–1781, https://doi.org/10.1007/s10346-017-0820-0, 2017b.~~

~~Steger, S., Mair, V., Kofler, C., Pittore, M., Zebisch, M., and Schneiderbauer, S.: Correlation does not imply geomorphic causation in data-driven landslide susceptibility modelling – Benefits of exploring landslide data collection effects, Sci. Total Environ., 776, 145935, https://doi.org/10.1016/j.scitotenv.2021.145935, 2021.~~

~~Tanyaş, H. and Lombardo, L.: Completeness Index for Earthquake-Induced Landslide Inventories, Eng. Geol., 264, 105331, https://doi.org/10.1016/j.enggeo.2019.105331, 2020.~~

~~Tanyaş, H., Westen, C. J. van, Allstadt, K. E., and Jibson, R. W.: Factors controlling landslide frequency–area distributions, Earth Surf. Process. Landf., 44, 900–917, https://doi.org/10.1002/esp.4543, 2019.~~

~~Taylor, F. E., Tarolli, P., and Malamud, B. D.: Preface: Landslide–transport network interactions, Nat. Hazards Earth Syst. Sci., 20, 2585–2590, https://doi.org/10.5194/nhess-20-2585-2020, 2020.~~

~~Tekin, S.: Completeness of landslide inventory and landslide susceptibility mapping using logistic regression method in Ceyhan Watershed (southern Turkey), Arab. J. Geosci., 14, 1706, https://doi.org/10.1007/s12517-021-07583-5, 2021.~~

~~Trigila, A., Iadanza, C., and Spizzichino, D.: Quality assessment of the Italian Landslide Inventory using GIS processing, Landslides, 7, 455–470, 2010.~~

~~Ubaidulloev, A., Kaiheng, H., Rustamov, M., and Kurbanova, M.: Landslide Inventory along a National Highway Corridor in the Hissar-Allay Mountains, Central Tajikistan, GeoHazards, 2, 212–227, https://doi.org/10.3390/geohazards2030012, 2021.~~

~~Van Den Eeckhaut, M. and Hervás, J.: State of the art of national landslide databases in Europe and their potential for assessing landslide susceptibility, hazard and risk, Geomorphology, 139–140, 545–558, https://doi.org/10.1016/j.geomorph.2011.12.006, 2012.~~

~~Voumard, J., Derron, M.-H., and Jaboyedoff, M.: Natural hazard events affecting transportation networks in Switzerland from 2012 to 2016, Nat. Hazards Earth Syst. Sci., 18, 2093–2109, https://doi.org/10.5194/nhess-18-2093-2018, 2018.~~

~~van Westen, C. J., Castellanos, E., and Kuriakose, S. L.: Spatial data for landslide susceptibility, hazard, and vulnerability assessment: An overview, Eng. Geol., 102, 112–131, https://doi.org/10.1016/j.enggeo.2008.03.010, 2008.~~

~~Wood, J. L., Harrison, S., Reinhardt, L., and Taylor, F. E.: Landslide databases for climate change detection and attribution, Geomorphology, 355, 107061, https://doi.org/10.1016/j.geomorph.2020.107061, 2020.~~

Con formato: Color de fuente: Negro

Con formato: Normal, Borde: Superior: (Sin borde), Inferior: (Sin borde), Izquierda: (Sin borde), Derecha: (Sin borde), Entre : (Sin borde), Punto de tabulación: 7,96 cm, Centrado + 15,92 cm, Derecha

~~Zhang, J., van Westen, C. J., Tanyas, H., Mavrouli, O., Ge, Y., Bajrachary, S., Gurung, D. R., Dhital, M. R., and Khanal, N. R.: How size and trigger matter: analyzing rainfall- and earthquake-triggered landslide inventories and their causal relation in the Koshi River basin, central Himalaya, Nat. Hazards Earth Syst. Sci., 19, 1789–1805, https://doi.org/10.5194/nhess-19-1789-2019, 2019a.~~

~~Zhang, T., Han, L., Han, J., Li, X., Zhang, H., and Wang, H.: Assessment of Landslide Susceptibility Using Integrated Ensemble Fractal Dimension with Kernel Logistic Regression Model, Entropy, 21, 218, https://doi.org/10.3390/e21020218, 2019b.~~Bera, S., Guru, B., and V, R.: Evaluation of landslide susceptibility models: A comparative study on the part of Western Ghat Region, India, Remote Sens. Appl. Soc. Environ., 13, 39–52, https://doi.org/10.1016/j.rsase.2018.10.010, 2019.

Bornaetxea, T. and Marchesini, I.: r.survey: a tool for calculating visibility of variable-size objects based on orientation, Int. J. Geogr. Inf. Sci., 0, 1–24, https://doi.org/10.1080/13658816.2021.1942476, 2021.

Bornaetxea, T., Rossi, M., Marchesini, I., and Alvioli, M.: Effective surveyed area and its role in statistical landslide susceptibility assessments, Nat. Hazards Earth Syst. Sci., 18, 2455–2469, https://doi.org/10.5194/nhess-18-2455-2018, 2018.

Brenning, A., Schwinn, M., Ruiz-Páez, A. P., and Muenchow, J.: Landslide susceptibility near highways is increased by 1 order of magnitude in the Andes of southern Ecuador, Loja province, Nat. Hazards Earth Syst. Sci., 15, 45–57, https://doi.org/10.5194/nhess-15-45-2015, 2015.

Cascini, L.: Applicability of landslide susceptibility and hazard zoning at different scales, Eng. Geol., 102, 164–177, https://doi.org/10.1016/j.enggeo.2008.03.016, 2008.

Chaparro-Cordón, J. L., Rodriguez, E. A., Florez, M. S. R., García-Delgado, H., and Enif Medina Bello: Statistical description of some landslide inventories from Colombian Andes: study cases in Mocoa, Villavicencio, Popayán, and Cajamarca, https://doi.org/10.13140/RG.2.2.17237.04327, 2020.

Corominas, J., van Westen, C., Frattini, P., Cascini, L., Malet, J.-P., Fotopoulou, S., Catani, F., van Den Eeckhaut, M., Mavrouli, O., Agliardi, F., Pitilakis, K., Winter, M. G., Pastor, M., Ferlisi, S., Tofani, V., Hervás, J., and Smith, J. T.: Recommendations for the quantitative analysis of landslide risk, Bull. Eng. Geol. Environ., 73, 209–263, https://doi.org/10.1007/s10064-013-0538-8, 2014.

Cova, T. J., Tsou Ming-Hsiang, Bareth Georg, Song Chunqiao, Song Yan, Cao Kai, and Silva Elisabete A: Comprehensive Geographic Information Systems, Elsevier, 2018.

Domingo-Santos, J. M., de Villarán, R. F., Rapp-Arrarás, Í., and de Provens, E. C.-P.: The visual exposure in forest and rural landscapes: An algorithm and a GIS tool, Landsc. Urban Plan., 101, 52–58, https://doi.org/10.1016/j.landurbplan.2010.11.018, 2011.

Donnini, M., Napolitano, E., Salvati, P., Ardizzone, E., Bucci, F., Fiorucci, F., Santangelo, M., Cardinali, M., and Guzzetti, F.: Impact of event landslides on road networks: a statistical analysis of two Italian case studies, Landslides, 14, 1521–1535, https://doi.org/10.1007/s10346-017-0829-4, 2017.

Con formato: Color de fuente: Negro

Con formato: Normal, Borde: Superior: (Sin borde), Inferior: (Sin borde), Izquierda: (Sin borde), Derecha: (Sin borde), Entre : (Sin borde), Punto de tabulación: 7,96 cm, Centrado + 15,92 cm, Derecha

Fell, R., Corominas, J., Bonnard, C., Cascini, L., Leroi, E., and Savage, W. Z.: Guidelines for landslide susceptibility, hazard and risk zoning for land-use planning, Eng. Geol., 102, 99–111, https://doi.org/10.1016/j.enggeo.2008.03.014, 2008.

Fiorucci, F., Giordan, D., Santangelo, M., Dutto, F., Rossi, M., and Guzzetti, F.: Criteria for the optimal selection of remote sensing optical images to map event landslides, Nat. Hazards Earth Syst. Sci., 18, 405–417, https://doi.org/10.5194/nhess-18-405-2018, 2018.

Fontani, F.: Application of the Fisher's "Horizon Viewshed" to a proposed power transmission line in Nozzano (Italy). Transactions in GIS, 21(4), 835-843, https://doi.org/10.1111/tgis.12260, 2017.

Fressard, M., Thiery, Y., and Maquaire, O.: Which data for quantitative landslide susceptibility mapping at operational scale? Case study of the Pays d'Auge plateau hillslopes (Normandy, France), Nat. Hazards Earth Syst. Sci., 14, 569–588, https://doi.org/10.5194/nhess-14-569-2014, 2014.

Galli, M., Ardizzone, F., Cardinali, M., Guzzetti, F., and Reichenbach, P.: Comparing landslide inventory maps, Geomorphology, 94, 268–289, https://doi.org/10.1016/j.geomorph.2006.09.023, 2008.

Gariano, S. L. and Guzzetti, F.: Landslides in a changing climate, Earth-Sci. Rev., 162, 227–252, https://doi.org/10.1016/j.earscirev.2016.08.011, 2016.

Ghorbanzadeh, O., Meena, S. R., Blaschke, T., and Aryal, J.: UAV-Based Slope Failure Detection Using Deep-Learning Convolutional Neural Networks, Remote Sens., 11, 2046, https://doi.org/10.3390/rs11172046, 2019.

Giordan, D., Hayakawa, Y., Nex, F., Remondino, F., and Tarolli, P.: Review article: the use of remotely piloted aircraft systems (RPASs) for natural hazards monitoring and management, Nat. Hazards Earth Syst. Sci., 18, 1079–1096, https://doi.org/10.5194/nhess-18-1079-2018, 2018.

Guzzetti, F., Carrara, A., Cardinali, M., and Reichenbach, P.: Landslide hazard evaluation: a review of current techniques and their application in a multi-scale study, Central Italy, Geomorphology, 31, 181–216, https://doi.org/10.1016/S0169-555X(99)00078-1, 1999.

Guzzetti, F., Reichenbach, P., Ardizzone, F., Cardinali, M., and Galli, M.: Estimating the quality of landslide susceptibility models, Geomorphology, 81, 166–184, https://doi.org/10.1016/j.geomorph.2006.04.007, 2006.

Guzzetti, F., Mondini, A. C., Cardinali, M., Fiorucci, F., Santangelo, M., and Chang, K.-T.: Landslide inventory maps: New tools for an old problem, Earth-Sci. Rev., 112, 42–66, https://doi.org/10.1016/j.earscirev.2012.02.001, 2012.

Hao, L., Rajaneesh A, van Westen, C., Sajinkumar K. S, Martha, T. R., Jaiswal, P., and McAdoo, B. G.: Constructing a complete landslide inventory dataset for the 2018 monsoon disaster in Kerala, India, for land use change analysis, Earth Syst. Sci. Data, 12, 2899–2918, https://doi.org/10.5194/essd-12-2899-2020, 2020.

Healey, C. G. and Sawant, A. P.: On the limits of resolution and visual angle in visualization, ACM Trans. Appl. Percept., 9, 20:1-20:21, https://doi.org/10.1145/2355598.2355603, 2012.

Hussain, G., Singh, Y., Singh, K., and Bhat, G. M.: Landslide susceptibility mapping along national highway-1 in Jammu and Kashmir State (India), Innov. Infrastruct. Solut., 4, 59, https://doi.org/10.1007/s41062-019-0245-9, 2019.

Con formato: Color de fuente: Negro

Con formato: Normal, Borde: Superior: (Sin borde), Inferior: (Sin borde), Izquierda: (Sin borde), Derecha: (Sin borde), Entre : (Sin borde), Punto de tabulación: 7,96 cm, Centrado + 15,92 cm, Derecha

Jacobs, L., Kervyn, M., Reichenbach, P., Rossi, M., Marchesini, I., Alvioli, M., and Dewitte, O.: Regional susceptibility assessments with heterogeneous landslide information: Slope unit- vs. pixel-based approach, Geomorphology, 356, 107084, https://doi.org/10.1016/j.geomorph.2020.107084, 2020.

Knevels, R., Petschko, H., Proske, H., Leopold, P., Maraun, D., and Brenning, A.: Event-Based Landslide Modeling in the Styrian Basin, Austria: Accounting for Time-Varying Rainfall and Land Cover, Geosciences, 10, 217, https://doi.org/10.3390/geosciences10060217, 2020.

Lee, S., Jang, J., Kim, Y., Cho, N., and Lee, M.-J.: Susceptibility Analysis of the Mt. Umyeon Landslide Area Using a Physical Slope Model and Probabilistic Method, Remote Sens., 12, 2663, https://doi.org/10.3390/rs12162663, 2020.

Lima, P., Steger, S., and Glade, T.: Counteracting flawed landslide data in statistically based landslide susceptibility modelling for very large areas: a national-scale assessment for Austria, Landslides, 18(11), 3531-3546, https://doi.org/10.1007/s10346-021-01693-7, 2021.

Malamud, B. D., Turcotte, D. L., Guzzetti, F., and Reichenbach, P.: Landslide inventories and their statistical properties, Earth Surf. Process. Landf., 29, 687–711, https://doi.org/10.1002/esp.1064, 2004.

Martha, T. R., Roy, P., Jain, N., Khanna, K., Mrinalni, K., Kumar, K. V., and Rao, P. V. N.: Geospatial landslide inventory of India—an insight into occurrence and exposure on a national scale, Landslides, 18, 2125–2141, https://doi.org/10.1007/s10346-021-01645-1, 2021.

McAdoo, B. G., Quak, M., Gnyawali, K. R., Adhikari, B. R., Devkota, S., Rajbhandari, P. L., and Sudmeier-Rieux, K.: Roads and landslides in Nepal: how development affects environmental risk, Nat. Hazards Earth Syst. Sci., 18, 3203–3210, https://doi.org/10.5194/nhess-18-3203-2018, 2018.

Meena, S. R., Mishra, B. K., and Tavakkoli Piralilou, S.: A Hybrid Spatial Multi-Criteria Evaluation Method for Mapping Landslide Susceptible Areas in Kullu Valley, Himalayas, Geosciences, 9, 156, https://doi.org/10.3390/geosciences9040156, 2019.

Melzner, S., Rossi, M., and Guzzetti, F.: Impact of mapping strategies on rockfall frequency-size distributions, Eng. Geol., 272, 105639, https://doi.org/10.1016/j.enggeo.2020.105639, 2020.

Meneses, B. M., Pereira, S., and Reis, E.: Effects of different land use and land cover data on the landslide susceptibility zonation of road networks, Nat. Hazards Earth Syst. Sci., 19, 471–487, https://doi.org/10.5194/nhess-19-471-2019, 2019.

Mondini, A. C., Viero, A., Cavalli, M., Marchi, L., Herrera, G., and Guzzetti, F.: Comparison of event landslide inventories: the Pogliaschina catchment test case, Italy, Nat. Hazards Earth Syst. Sci., 14, 1749–1759, https://doi.org/10.5194/nhess-14-1749-2014, 2014.

Nicu, I. C., Lombardo, L., and Rubensdotter, L.: Preliminary assessment of thaw slump hazard to Arctic cultural heritage in Nordenskiöld Land, Svalbard, Landslides, 18, 2935–2947, https://doi.org/10.1007/s10346-021-01684-8, 2021.

Park, J.-Y., Lee, S.-R., Lee, D.-H., Kim, Y.-T., and Lee, J.-S.: A regional-scale landslide early warning methodology applying statistical and physically based approaches in sequence, Eng. Geol., 260, 105193, https://doi.org/10.1016/j.enggeo.2019.105193, 2019.

36

Con formato: Color de fuente: Negro

Con formato: Normal, Borde: Superior: (Sin borde), Inferior: (Sin borde), Izquierda: (Sin borde), Derecha: (Sin borde), Entre : (Sin borde), Punto de tabulación: 7,96 cm, Centrado + 15,92 cm, Derecha

Piacentini, D., Troiani, F., Daniele, G., and Pizziolo, M.: Historical geospatial database for landslide analysis: the Catalogue of Landslide OCcurrences in the Emilia-Romagna Region (CLOCkER), Landslides, 15, 811–822, https://doi.org/10.1007/s10346-018-0962-8, 2018.

Reichenbach, P., Rossi, M., Malamud, B. D., Mihir, M., and Guzzetti, F.: A review of statistically-based landslide susceptibility models, Earth-Sci. Rev., 180, 60–91, https://doi.org/10.1016/j.earscirev.2018.03.001, 2018.

Roberts, S., Jones, J. N., and Boulton, S. J.: Characteristics of landslide path dependency revealed through multiple resolution landslide inventories in the Nepal Himalaya, Geomorphology, 390, 107868, https://doi.org/10.1016/j.geomorph.2021.107868, 2021.

Rohan, T. and Shelef, E.: Analysis of 311 based Landslide Inventories for Landslide Susceptibility Mapping, AGU Fall Meet. Abstr., 33, 2019.

Santangelo, M., Marchesini, I., Bucci, F., Cardinali, M., Fiorucci, F., and Guzzetti, F.: An approach to reduce mapping errors in the production of landslide inventory maps, Nat. Hazards Earth Syst. Sci., 15, 2111–2126, https://doi.org/10.5194/nhess-15-2111-2015, 2015.

Sidle, R. C. and Ziegler, A. D.: The dilemma of mountain roads, Nat. Geosci., 5, 437–438, https://doi.org/10.1038/ngeo1512, 2012.

Sidle, R. C., Ghestem, M., and Stokes, A.: Epic landslide erosion from mountain roads in Yunnan, China – challenges for sustainable development, Nat. Hazards Earth Syst. Sci., 14, 3093–3104, https://doi.org/10.5194/nhess-14-3093-2014, 2014.

Stark, C. P. and Hovius, N.: The characterization of landslide size distributions, Geophys. Res. Lett., 28, 1091–1094, https://doi.org/10.1029/2000GL008527, 2001.

Steger, S., Brenning, A., Bell, R., Petschko, H., and Glade, T.: Exploring discrepancies between quantitative validation results and the geomorphic plausibility of statistical landslide susceptibility maps, Geomorphology, 262, 8–23, https://doi.org/10.1016/j.geomorph.2016.03.015, 2016a.

Steger, S., Brenning, A., Bell, R., and Glade, T.: The propagation of inventory-based positional errors into statistical landslide susceptibility models, Nat. Hazards Earth Syst. Sci., 16, 2729–2745, https://doi.org/10.5194/nhess-16-2729-2016, 2016b.

Steger, S., Brenning, A., Bell, R., and Glade, T.: The influence of systematically incomplete shallow landslide inventories on statistical susceptibility models and suggestions for improvements, Landslides, 14, 1767–1781, https://doi.org/10.1007/s10346-017-0820-0, 2017.

Steger, S., Mair, V., Kofler, C., Pittore, M., Zebisch, M., and Schneiderbauer, S.: Correlation does not imply geomorphic causation in data-driven landslide susceptibility modelling – Benefits of exploring landslide data collection effects, Sci. Total Environ., 776, 145935, https://doi.org/10.1016/j.scitotenv.2021.145935, 2021.

Tanyaş, H., Görüm, T., Kirschbaum, D., and Lombardo, L.: Could road constructions be more hazardous than an earthquake in terms of mass movement?, Natural Hazards, 1-25, https://doi.org/10.1007/s11069-021-05199-2, 2022.

Con formato: Color de fuente: Negro

Con formato: Normal, Borde: Superior: (Sin borde), Inferior: (Sin borde), Izquierda: (Sin borde), Derecha: (Sin borde), Entre : (Sin borde), Punto de tabulación: 7,96 cm, Centrado + 15,92 cm, Derecha

Tanyaş, H. and Lombardo, L.: Completeness Index for Earthquake-Induced Landslide Inventories, Eng. Geol., 264, 105331, https://doi.org/10.1016/j.enggeo.2019.105331, 2020.

Tanyaş, H., Westen, C. J. van, Allstadt, K. E., and Jibson, R. W.: Factors controlling landslide frequency–area distributions, Earth Surf. Process. Landf., 44, 900–917, https://doi.org/10.1002/esp.4543, 2019.

Taylor, F. E., Tarolli, P., and Malamud, B. D.: Preface: Landslide–transport network interactions, Nat. Hazards Earth Syst. Sci., 20, 2585–2590, https://doi.org/10.5194/nhess-20-2585-2020, 2020.

Tekin, S.: Completeness of landslide inventory and landslide susceptibility mapping using logistic regression method in Ceyhan Watershed (southern Turkey), Arab. J. Geosci., 14, 1706, https://doi.org/10.1007/s12517-021-07583-5, 2021.

Trigila, A., Iadanza, C., and Spizzichino, D.: Quality assessment of the Italian Landslide Inventory using GIS processing, Landslides, 7, 455–470, 2010.

Ubaidulloev, A., Kaiheng, H., Rustamov, M., and Kurbanova, M.: Landslide Inventory along a National Highway Corridor in the Hissar-Allay Mountains, Central Tajikistan, GeoHazards, 2, 212–227, https://doi.org/10.3390/geohazards2030012, 2021.

van Den Eeckhaut, M. and Hervás, J.: State of the art of national landslide databases in Europe and their potential for assessing landslide susceptibility, hazard and risk, Geomorphology, 139–140, 545–558, https://doi.org/10.1016/j.geomorph.2011.12.006, 2012.

Voumard, J., Derron, M.-H., and Jaboyedoff, M.: Natural hazard events affecting transportation networks in Switzerland from 2012 to 2016, Nat. Hazards Earth Syst. Sci., 18, 2093–2109, https://doi.org/10.5194/nhess-18-2093-2018, 2018.

van Westen, C. J., Castellanos, E., and Kuriakose, S. L.: Spatial data for landslide susceptibility, hazard, and vulnerability assessment: An overview, Eng. Geol., 102, 112–131, https://doi.org/10.1016/j.enggeo.2008.03.010, 2008.

Zhang, T., Han, L., Han, J., Li, X., Zhang, H., and Wang, H.: Assessment of Landslide Susceptibility Using Integrated Ensemble Fractal Dimension with Kernel Logistic Regression Model, Entropy, 21, 218, https://doi.org/10.3390/e21020218, 2019.

Con formato: Fuente: Times New Roman

Con formato: Sangría: Izquierda: 0 cm, Primera línea: 0 cm

Con formato: Color de fuente: Negro

Con formato: Normal, Borde: Superior: (Sin borde), Inferior: (Sin borde), Izquierda: (Sin borde), Derecha: (Sin borde), Entre : (Sin borde), Punto de tabulación: 7,96 cm, Centrado + 15,92 cm, Derecha